Journal of Nanobiotechnology

RESEARCH Open Access

Baicalein based nano-delivery system restores mitochondrial homeostasis through PPAR signaling pathway to promote wound healing in diabetes

Danlei Qin[1,2], Weiting Hu[3], Yanqin Guo[4], Rui Cheng[5], Fengxiang Hao[1] and Bin Zhao[1*]

Abstract

Wound healing in diabetes is a substantial clinical challenge due to the hyperglycemic microenvironment, high pH, bacterial infection, persistent inflammation, and impaired cellular functions, attributed to mitochondrial dysfunction. Here, we have developed an injectable photo-crosslinking nanocomposite hydrogel (BA/GOx@ZIF-8@GelMA, BGZ@GelMA) with baicalein (BA) and glucose oxidase (GOx) loaded Zinc metal-organic framework (ZIF-8) based on methacrylated gelatin (GelMA) to accelerate diabetic infected wound healing by regulating subcellular and cellular functions. The combination of ZIF-8 and BA gives the hydrogel excellent antibacterial properties. A high blood sugar environment triggers the release of GOx in BGZ@GelMA, reducing local glucose and pH, producing hydrogen peroxide (H_2O_2), and releasing BA and Zinc ions (Zn^{2+}). This process provides a suitable microenvironment for wound healing. Zn^{2+} can significantly inhibit the proliferation of *Staphylococcus aureus* (*S.aureus*) and *Escherichia coli* (*E.coli*). The released BA can clear ROS in cells and mitochondria, restore mitochondrial function and stability, and make the hydrogel fundamentally improve the cell function damage induced by hyperglycemia, and ultimately promote cell proliferation, migration and angiogenesis. In general, our multifunctional nanocomposite hydrogel provides a new strategy for diabetes wound healing at the subcellular and cellular functional levels.

Keywords Baicalein, Metal-organic framework, Mitochondrion, Diabetic wound healing

Introduction

Diabetes wound is one of the complications of diabetes, which seriously affects the quality of life of patients and increases their burden of life [1, 2]. Hyperglycemia is an essential factor affecting wound healing [3]. Firstly, the hyperglycemia microenvironment can provide excess nutrients for bacteria to proliferate, resulting in persistent bacterial infection in the wound and aggravating the inflammatory response [4]; Secondly, abnormal glucose metabolism in the wound can cause oxidative stress [5], inducing mitochondrial dysfunction and cell apoptosis in endothelial cells, inhibiting migration and proliferation of fibroblast, ultimately leading to dysfunction of the vascular and poor regeneration, resulting in wound ischemia, hypoxia, and delayed healing [6, 7]. Therefore, remodeling the high-glycemic and persistent inflammatory microenvironment is an important challenge, inhibiting bacterial infection, and promoting angiogenesis to accelerate diabetic wound healing [8]. Currently, diabetic wounds are treated in a single way, and given the complexity of diabetic wound healing, there is an urgent

*Correspondence:
Bin Zhao
sxmu0688@126.com

Full list of author information is available at the end of the article

Graphical abstract

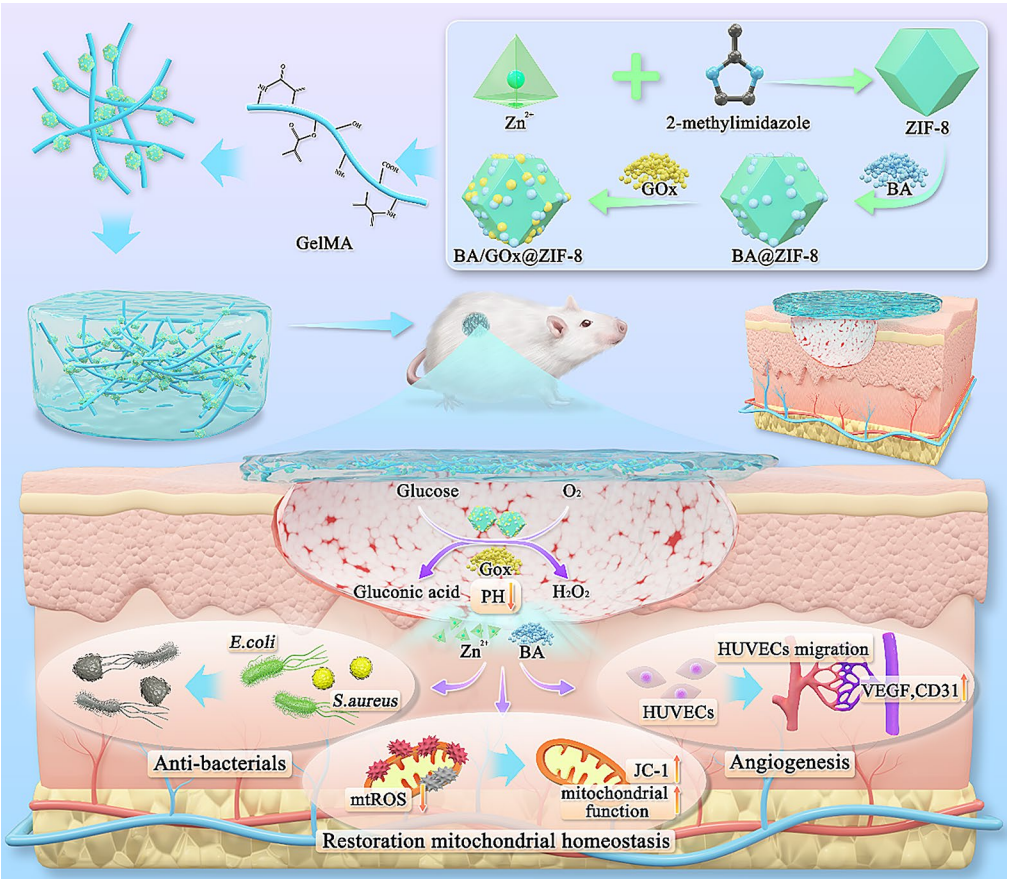

need to develop multifunctional biomaterials to salvage impaired cellular functions in the hyperglycemia microenvironment [9]. In recent years, multifunctional hydrogels have gained widespread attention due to their drug delivery, anti-inflammatory and antibacterial capabilities [10–12]. Its special porous structure and swelling properties give hydrogels a unique advantage in wound healing applications [13]. Therefore, in this study, we developed an injectable photo-crosslinked nanocomposite hydrogel and explored its properties and mechanism of action for chronic diabetic wounds.

Localized high glucose levels are the most critical problem in diabetic wounds and a pressing scientific issue. GOx is a natural enzyme that has attracted great research interest in the biomedical field due to its good biocompatibility, non-toxicity, and unique glucose-catalyzing properties [14]. GOx has been exploited for glucose depletion in starvation treatments [15], and Tian et al. found that GOx-loaded antimicrobial hydrogel reduces local blood glucose, inhibits the inflammatory response, and promotes immunomodulation to accelerate the healing of bacterially infected wounds [16]. GO_X catalyzes glucose to produce gluconic acid and hydrogen peroxide (H_2O_2) and is considered a candidate enzyme to regulate the high glucose microenvironment of diabetes wounds [14]. Delivering GOx to the wound site can reduce local glucose concentration and pH value, thereby activating the pH response system. In addition, the generated H_2O_2 and its metabolites hydroxyl radicals can damage bacterial cell components, leading to the rupture of bacterial cell membranes and walls and exerting antibacterial effects [17, 18]. However, GOx alone cannot meet the dynamic needs of diabetes wound healing.

Excessive oxidative stress can also seriously hinder wound healing [19–21], but the related cellular and organelle changes have not received sufficient attention. Mitochondria are dynamic cross-linked organelles with a network structure and are the main source of ROS in cells [22]. However, ROS in turn stimulates mitochondrial dysfunction. Traditional Chinese medicine's antioxidant and anti-inflammatory properties and its active ingredients have been widely studied [23–25]. Among these natural compounds, BA is a flavonoid compound isolated from the root of Scutellaria baicalensis, which has antibacterial

[26], anti-inflammatory [27], antioxidant, anti-aging, and liver protective properties. Research has found that baicalein can alleviate oxidative stress-induced liver damage by regulating the KLF4-Mrach5-Drp1 signaling pathway to maintain mitochondrial functional homeostasis [28]. However, despite the excellent pharmacological properties of BA, its poor solubility and low bioavailability limit its application, thus requiring the development of more efficient and reliable drug delivery systems [29]. Zinc-based metal-organic frameworks (Zn-MOFs) are a novel antibacterial nanomaterial with a porous structure, capable of drug loading [30], enzyme immobilization [31], and acid-reactive drug release [32]. In the microenvironment of diabetes, local glucose is catalyzed by GOx to produce glucuronic acid to reduce the pH value of the wound, and the decomposition of Zn-MOFs enables the continuous release of Zn^{2+}. In addition to playing an antibacterial role, it has been reported that Zn^{2+} can effectively restore the glycolysis OXPHOS imbalance, restore cell bioenergy, alleviate oxidative damage, rescue damaged mitochondria, and inhibit the production of inflammatory factors by regulating the AKT/GSK3β/NRF-2 pathway [33]. Therefore, slowing down the oxidative stress on the wound surface and protecting the mitochondrial function will be an innovative treatment strategy for diabetes chronic wounds, and can also guide the design of biomaterials for diabetes wound repair.

Here, we prepared a methacrylate gelatin (GelMA) hydrogel patch loaded with BA and GOx in ZIF-8 nanoparticles (BA/GOx@ZIF-8) (Scheme 1). Loading BA and GOx onto ZIF-8 can avoid the instability of GOx enzyme, the low water solubility of free BA, and limited bioavailability. GOx has the catalytic ability to consume glucose and produce H_2O_2 in the wound area of diabetes, improving the high glucose microenvironment of the wound; Meanwhile, under the synergistic effect of Zn^{2+}, the generated H_2O_2 can effectively inhibit bacterial growth; The natural active ingredient BA effectively alleviates oxidative stress and inflammatory reactions at the wound site by protecting mitochondrial function. Therefore, GOx, $Zn^{2+}$and BA play an important and positive role in all stages of wound healing in diabetes. These nanoparticles are loaded into injectable photo-cross-linked GelMA hydrogel, which is similar to the extracellular matrix (ECM) and has good biocompatibility. The three-dimensional (3D) network of hydrogel supports the continuous release of nanoparticles, thus enhancing the antioxidant and immune inflammatory regulation

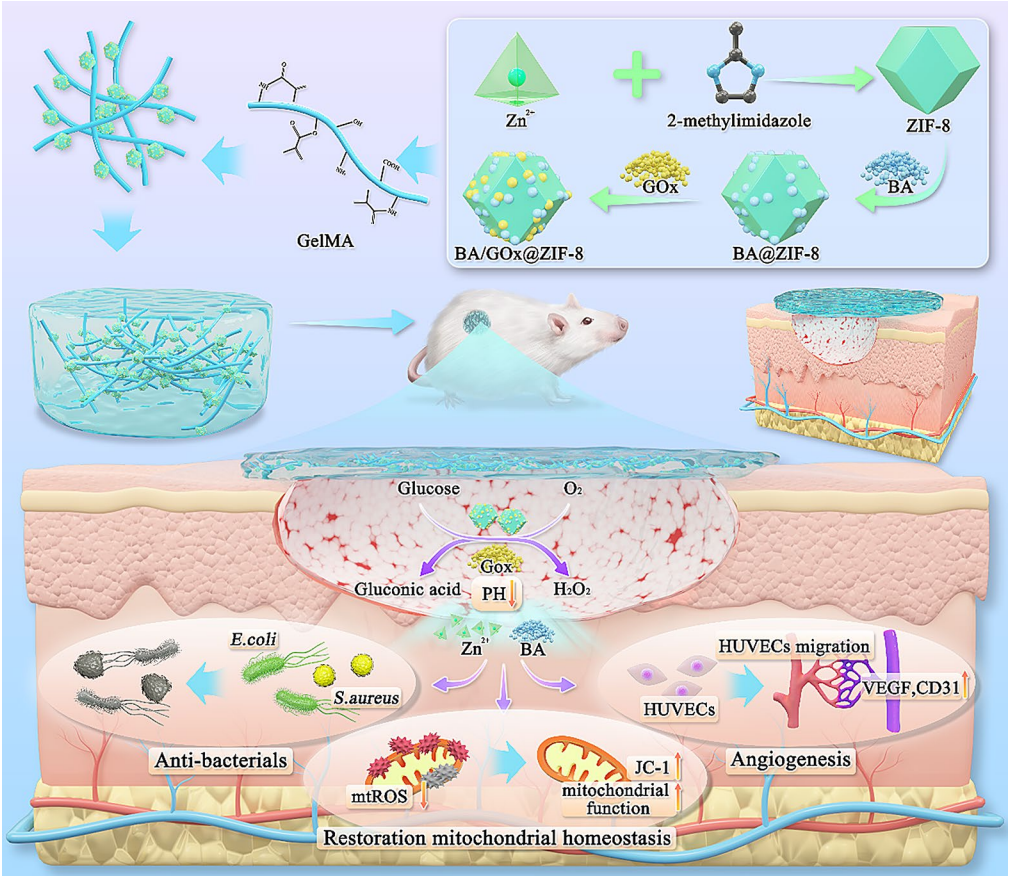

Scheme 1 Schematic diagram for the preparation of nanocomposite hydrogel and its function mechanism in diabetic wound treatment

performance. Because of its porous structure, it is conducive to the gas exchange at the wound site, isolating external bacteria, and forming a good physical barrier. In addition, these injectable hydrogels offer the advantages of minimally invasive and precision targeting, in situ adaptability, dynamic tunability and stability, providing a comprehensive solution for chronic diabetic wounds [34, 35]. In this study, BA/GOx@ZIF-8 Gel (BGZ@GelMA) hydrogel provides an innovative strategy, which can reverse the mitochondrial dysfunction and angiogenesis disorder caused by hyperglycemia, alleviate the oxidative stress at the wound site, significantly inhibit bacterial growth, and finally make the diabetes wound heal well.

Materials and methods

Preparation of ZIF-8, BA@ZIF-8, and BA/GOx@ZIF-8 nanoparticles and GelMA hydrogel

The synthesis method of ZIF-8, BA@ZIF-8, and BA/GOx@ZIF-8 nanoparticles follows our previous research. In brief, 2-mIM (300 mg) was dispersed in a methanol solution (10 mL) and Zn $(NO_3)2{\cdot}6H_2O$ (150 mg) was dissolved in a methanol solution (20 mL). After stirring both solutions until clear, quickly pour Zn $(NO_3)2{\cdot}6H_2O$ solution into 2-mIM solution and let it react for 3 h. Following centrifugation (10,000 rpm for 5 min), the milky white solids were collected and washed, then dried at 60 °C overnight under vacuum to remove any remaining solvents. Following the same method, Add BA (1 mg/mL) and GOx (100 μg/mL) separately to the ZIF-8 solution to obtain BA@ZIF-8 and BA/GOx@ZIF-8.

The first step was to synthesize GelMA based on previously published reports [31]. Briefly, 1 g of gelatin was dissolved in 10 mL of phosphate-buffered saline (PBS) solution at 50 °C, followed by adding 0.8 mL of methacrylic anhydride and stirring for 3 h. The reaction solution was transferred to a dialysis membrane (7000 kDa), dialyzed in deionized water for 5 days, and then lyophilized to obtain GelMA sponge. Add a certain concentration of ZIF-8, BA@ZIF-8, and BA/GOx@ZIF-8 to the GelMA precursor solution, then introduce the photocrosslinking agent 0.1% LAP, which is crosslinked under visible light (405 nm, 25mW/cm^2, 30s) irradiation to obtain Z@GelMA, BZ@GelMA, and BGZ@GelMA hydrogel.

ZIF-8, BA@ZIF-8, and BA/GOx@ZIF-8 were imaged by scanning electron microscopy (SEM, JSM-7001F, Japan). X-ray diffraction (XRD) was measured on a Bruker D8 Advance device at Cu Kα (λ = 0.154056 nm) with a scanning rate of 10 min^{-1} in the 2θ range of 10–80°. The functional groups of the samples were further analyzed using a Fourier transform infrared (FTIR) spectrometer (Nicolet iS50, ThermoFisher, USA) at wavelengths ranging from 4000 to 400 cm^{-1}. The average particle size was measured by Zeta sizer. Zeta potential meter is used to detect the Zeta potential of the prepared sample.

Cell culture

Fibroblasts L929 and Human umbilical vein endothelial cells (HUVECs) were purchased from the Cell Bank of the Chinese Academy of Sciences (Shanghai, China) and cultured in Dulbecco's Modified Eagle's Medium (DMEM, Gabico) supplemented with 10% FBS and 1% dual antibody at 37 °C in a humidified incubator containing 5% CO_2.

Biocompatibility of the hydrogel

In vitro, adding LPS (1 μg/mL) and high glucose (33 mM) to the culture medium induces a high glucose inflammatory microenvironment. The cytotoxicity of different nanocomposite hydrogels (Z@GelMA, BZ@GelMA, and BGZ@GelMA) in HUVECs was evaluated by CCK-8 assay. First, the hydrogel precursor solutions loaded with different concentrations of ZIF-8, BA@ZIF-8, and BA/GOx@ZIF-8 (0,10, 20, 40, 60, 80, 100, 150, 200 μg/mL) were injected into the 96-well plate and then crosslinked with visible light. The HUVECs were seeded into 96-well plates at a density of 5×10^3 cells per well and cultured for 24 h. Subsequently, 10 μL CCK-8 reagent was added directly into each well under light-avoidance conditions. After the cells were put into the cell culture incubator for 2 h, the OD value at 450 nm was measured by the microplate reader (Thermofisher, USA).

HUVECs (2×10^4 cells/well) and L929 (2×10^4 cells/well) were seeded in 48-well plates overnight in the medium. Afterward, the cells were co-cultured with Z@GelMA, BZ@GelMA, and BGZ@GelMA hydrogel extracts for 1 d, 3 d, and 5 d. CCK-8 reagent was added to each well and incubated for 2 h. The measurement of absorbance at 450 nm was conducted for each well.

HUVECs and L929 were seeded in a 24-well plate and co-cultured with Z@GelMA, BZ@GelMA, and BGZ@GelMA hydrogel extracts for 3 days. HUVECs and L929 cells were exposed to live and dead dyes (500 μL per well, comprising 2 μM calcein and 8 μM propidium iodide at 37℃ for 40 min. The viability of cells (green) and dead cells (red) was visualized using an inverted fluorescence microscope.

Cell flow cytometry: HUVECs were seeded in a 6-well plate and co-cultured with Z@GelMA, BZ@GelMA, and BGZ@GelMA hydrogel extracts for 24 h. Subsequently, apoptosis in cells was evaluated through the Annexin V-FITC/PI Kit.

EDU cell proliferation assay: About 2×10^4 HUVECs were grown in 24-well plates and cultured with different nanocomposite hydrogel (Z@GelMA, BZ@GelMA, and BGZ@GelMA) at 37℃ for 24 h. After that, the cells were treated with 10 μM EDU (5-bromo-2-deoxyuracil)

reagent at 37℃ for 2 h, followed by fixation, permeabilization, and sequential staining with EDU and DAPI. EDU staining was observed using a laser confocal microscope (CLSM, Olympus, Japan). The proportion of HUVECs incorporating EDU was quantified using image J.

Ki-67 staining: HUVECs were inoculated into 24-well plates and co-cultured with Z@GelMA, BZ@GelMA, and BGZ@GelMA hydrogel extracts in a high-glucose inflammatory environment for 24 h. Cells were then fixed with 4% paraformaldehyde for 30 min, incubated with 0.1% Triton-X-100, and then blocked with 5% BSA for 30 min before staining with anti-Ki-67 antibody at 4℃ overnight. The next day, the cells were incubated with the corresponding fluorescent secondary antibodies for 1 h. The nucleus was labeled with DAPI (Solarbio, China), respectively. The cells were observed with CLSM.

Fresh mouse blood was collected for a blood compatibility test, and whole blood was washed and diluted into 5% (V/V) erythrocyte suspension with PBS. The hydrogel samples (GelMA, Z@GelMA, BZ@GelMA, and BGZ@GelMA) were incubated with erythrocyte suspension at 37 °C for 4 h and centrifuged for 5 min. The absorbance at 540 nm of the supernatant was measured using a microplate reader (Thermofisher, USA).

In vitro antimicrobial activity of hydrogel

S. aureus and *E. coli* were selected as bacterial models to evaluate the antibacterial activity of the hydrogels. Pre-position 200 μL of different nanocomposite hydrogels (Z@GelMA, BZ@GelMA, and BGZ@GelMA) on a 48-well plate, then a 1×10^5 CFU mL^{-1} bacterial suspension was added into the preloaded nanocomposite hydrogel. The 48-well plates were incubated at 37 °C for 24 h. After incubation, the bacterial solution was diluted and inoculated on a solid medium. Photographs were taken of the experimental results and the inhibition rate was calculated. Live/dead staining was conducted by coculturing materials with *S. aureus* and *E. coli* suspension (10^8 CFU/mL) for 6 h. The bacteria were collected through centrifugation and further stained with the live/dead SYTO9/PI bacterial viability kit. The results were recorded using a CLSM. The SEM image was applied to examine the morphology change of bacteria. Hydrogels were co-cultured with the bacterial suspension (2mL, 1.5×10^8 CFU mL^{-1}) of *S. aureus* and *E. coli* for 24 h at 37 °C. The bacteria were collected by centrifugation and fixed on a glass slide with 2.5% glutaraldehyde solution for 30 min. Samples were sequentially dehydrated in graded ethanol (30, 50, 75, 85, 90, 95, and 100%; 15 min each). Next, the specimens were air-dried and coated with gold. Ultimately, pictures were recorded by SEM at 20 kV. The inhibition and clearance effects of different hydrogels on bacterial biofilms were evaluated by crystal violet staining, and bacterial uptake of propidium iodide experiments were conducted to further demonstrate that Zn^{2+} and BA can damage bacterial membranes.

Detection of intracellular and mitochondrial ROS

DCFH-DA (S0033S, Beyotime, China) and MitoSOX (S0061S, Beyotime, China) were used to determine the levels of ROS present in cellular and mitochondrial, respectively. In vitro, adding LPS (1 μg/mL) and high glucose (33 mM) to the culture medium induces a high glucose inflammatory microenvironment. HUVECs were seeded into 6-well culture plates to attain around 80% confluency under different experimental conditions (Z@Gel, BZ@Gel, and BGZ@Gel nanocomposite hydrogel extracts), washed with PBS 3 times, and then the DCFH-DA (10 mM) or MitoSOX (0.1 μM) probe was loaded into the cells and incubated for 30 min at 37 °C. Cells were washed three times with PBS following incubation, and examined with a fluorescence microscope. Mito-tracker (0.1 μM) was stained to determine the mitochondrial position when detecting MitoSOX. Image J software was used to quantify fluorescence signal intensity.

Afterward, the mitochondrial membrane potential (MMP) of HUVECs cells was evaluated using a specific assay kit along with a JC-1 assay kit, following the provided instructions. HUVCEs were incubated with JC-1 ΔΨm probes (C2006, Beyotime, China) for 20 min at 37 °C in the dark and observed under a fluorescence microscope. The red/green fluorescence ratio was quantitatively analyzed to assess the change in ΔΨm using Image J software.

Cell scratching assay

Initially, HUVECs and L929 cells were seeded into the 6-well plate, and the cell layers were scratched by a 200 μL plastic pipette tip and then washed with PBS when reaching about 90%concourse. Subsequently, cells were continuously co-cultured with Z@GelMA, BZ@GelMA, and BGZ@GelMA hydrogel extracts in a high-glucose inflammatory environment. Photographs were taken at 0 h and 24 h to observe the migration of the cells. Image J was used for quantitative analysis of scratches. The area of each group of scratches at 0 h was recorded as S0, and after 24 h of intervention, the remaining area was measured and recorded as S1. The healing rate of scratches was calculated using the following formula: Scratch healing rate (%) = (S0-S1)/S0*100.

Cellular migration assay

We evaluated the migratory capacity of HUVECs and L929 using 8-μm pore size Transwell chambers. In short, HUVECs and L929 cells (5×10^4 cells per well) were cultured in the upper chamber, while the lower chamber was high sugar inflammatory DMEM complete medium containing Z@GelMA, BZ@GelMA and BGZ@GelMA

hydrogels. After 24 h of co-culture, the cells in the upper chamber that had not migrated were then carefully removed. Then the cells were fixed with 4% paraformaldehyde for 20 min and stained with 0.1% crystal violet for 20 min. The migration of the cells was subsequently observed and documented using a fluorescence microscope.

Tube formation experiment

Before cell seeding, 50 μL of Matrigel was applied onto the bottom of each well in the 96-well plate, followed by incubation for 30 min at 37 °C to ensure Matrigel solidification. HUVECs (2×10^4 cells/well) were subsequently seeded onto the Matrigel-coated substrates and cultured with high-glucose and LPS DMEM infused with extracts from Z@GelMA, BZ@GelMA, and BGZ@GelMA, alongside a complete medium serving as the control. After a 6 h incubation period at 37 °C in a culture incubator, the representative cellular images were captured using microscopy. The number of tube junctions was calculated using the angiogenesis plugin available from Image J.

Immunofluorescence staining assay

HUVECs were inoculated into 24-well plates and co-cultured with Z@GelMA, BZ@GelMA, and BGZ@GelMA hydrogel extracts in a high-glucose inflammatory environment for 24 h. Cells were then fixed with 4% paraformaldehyde for 30 min, incubated with 0.1% Triton-X-100, and then blocked with 5% BSA for 30 min before staining with anti-vascular endothelial growth factor (VEGF) and anti-CD31 antibody at 4 °C overnight. The next day, the cells were incubated with the corresponding fluorescent secondary antibodies for 1 h. The cytoskeleton and nucleus were labeled with TRITC-phalloidin (Solarbio, China) and DAPI (Solarbio, China), respectively. The cells were observed with CLSM and photographed.

Western blot (WB)

HUVECs were seeded into 6-well plates for 12 h, and exposed to a high-glycemic inflammatory environment. Subsequently, the cells were co-cultured with Z@GelMA, BZ@GelMA, and BGZ@GelMA hydrogel extracts for 24 h. The control group received no treatment. Protein extraction from the cells was performed by Total Protein Extraction Kit. The WB method follows the procedures of electrophoresis, membrane transfer, blocking, incubation of primary antibody, incubation of secondary antibody, and imaging. The antibodies are as follows: anti-VEGF and anti-β-actin. Use image J to analyze the grayscale values of different bands and perform quantitative analysis.

Transcriptome sequencing

The entire transcriptome sequencing of HUVECs treated with or without BGZ@GelMA was performed to investigate the mechanisms that promote wound healing.

Diabetic skin wound healing in vivo

All animal experiments were approved by the Ethics Committee of the School of Stomatology, Shanxi Medical University. Male Sprague-Dawley (SD) rats, four weeks old (weighting 150–200 g), the SD rat diabetic model was induced with streptozotocin (STZ, 50 mg/kg) for 3 days. Successful induction of diabetes is confirmed when blood glucose levels remain above 16.7 mmol/L for more than 4 weeks were used as research subjects. Thereafter, a round, full-thickness skin wound (diameter: 20 mm) was then made on the back skin of the diabetic rats. The rats were then randomly divided into three groups (each comprising 6 rats): Control, GelMA, and BGZ@GelMA. Use a camera to take photos of the wound area on days 0, 5, 10, 14, and 21, and use ImageJ to quantitatively analyze the wound healing situation. On days 7 and 21, residual wound tissue was collected, fixed with 4% paraformaldehyde, then inserted into paraffin and cut vertically into 5-μm-thick longitudinal sections. Inflammation and collagen deposition in the wounds were assessed using H&E staining and Masson staining. Immunohistochemical staining was used to assess IL-6, TNF-α, VEGF, and CD31 expression in the skin of each group to evaluate wound inflammation, angiogenesis, and tissue proliferation and repair. Quantitative analysis of immunohistochemical staining indicators using Image J.

Statistical analysis

All quantitative data were repeated at least three times and expressed as mean ± standard deviation. GraphPad Prism 8.0 and Origin Software were used for statistics and analysis. The experimental data between the two groups was compared using the student-t test. One-way ANOVA with Tukey's multiple comparison test was used to compare differences between the multiple groups. Statistical significance was set at: $^{*}p < 0.05$, $^{**}p < 0.01$, $^{***}p < 0.001$, and $^{****}p < 0.0001$.

Results and discussion

Characterization of the nanoparticles and hydrogel

Figure 1A shows the schematic illustration of the synthesis of BA/GOx@ZIF-8 nanoparticles and BGZ@GelMA nanocomposite hydrogels. The morphology of the sample was characterized by SEM (Fig. 1B). The results indicate that the representative SEM of ZIF-8 exhibits a regular dodecahedral structure, consistent with literature reports [36], with a diameter of approximately 150 nm. However, the diameter of ZIF-8 gradually increased to about 180 nm after loading BA and GOx

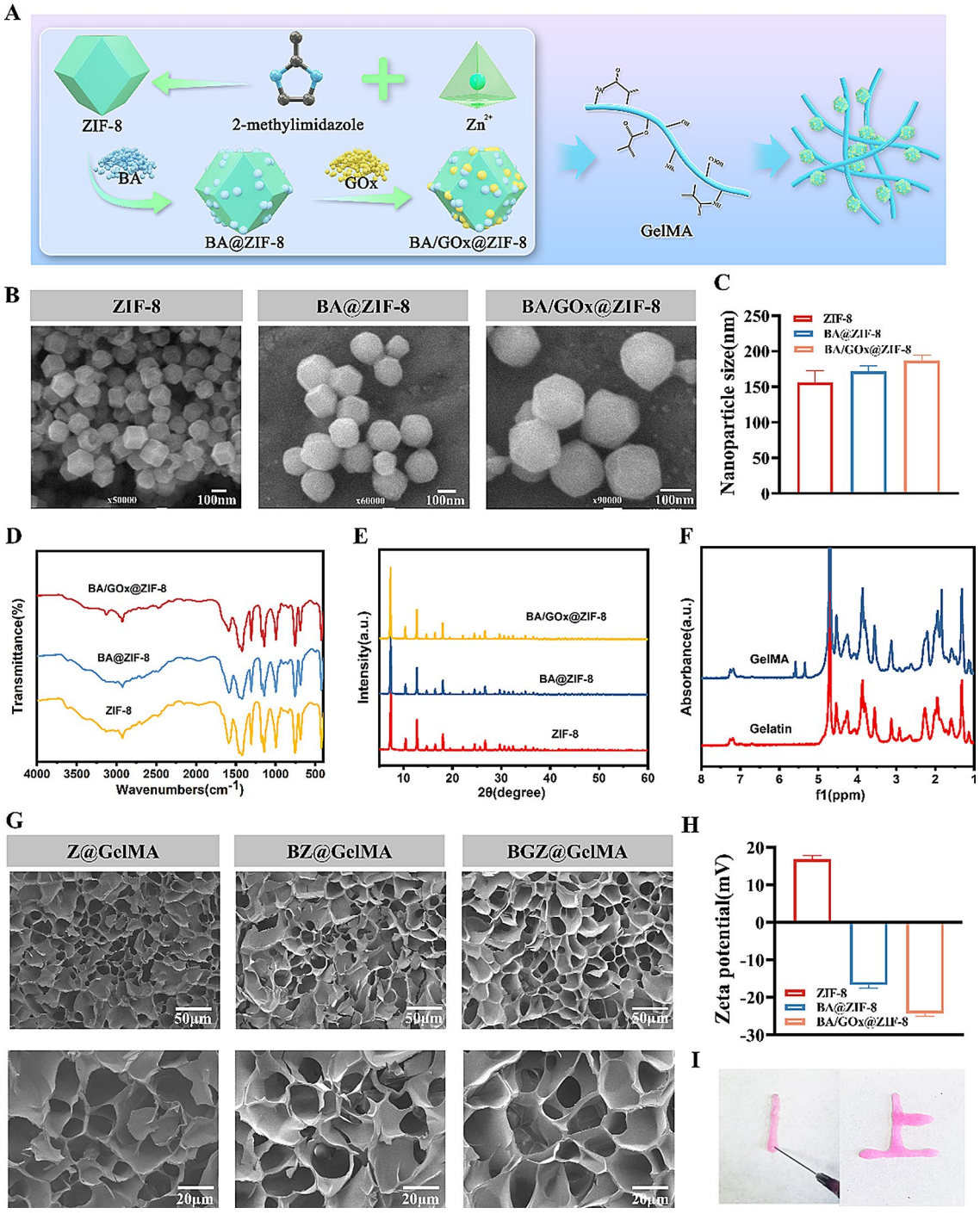

Fig. 1 Characterization of the nanocomposite hydrogel. (**A**) Schematic diagram of synthesis of nanoparticles and hydrogels. (**B**) SEM images of ZIF-8, BA@ZIF-8, and BA/GOx@ZIF-8 nanoparticles. (**C**) Nanoparticle size analysis of the ZIF-8, BA@ZIF-8, BA/GOx@ZIF-8. (**D**) FTIR spectra of the ZIF-8, BA@ZIF-8, and BA/GOx@ZIF-8 nanoparticles. (**E**) XRD spectra of ZIF-8, BA@ZIF-8, and BA/GOx@ZIF-8 nanoparticles. (**F**) ^{1}H NMR spectra of the GelMA and gelatin. (**G**) SEM images of the nanocomposite hydrogel. (**H**) Zeta potential of the ZIF-8, BA@ZIF-8, and BA/GOx@ZIF-8 nanoparticles. (**I**) The images of injectability of hydrogel

(Fig. 1C). Compared with the homogeneous dodecahedral structure of ZIF-8, the surfaces of BA@ZIF-8 and BA/GOx@ZIF-8 are slightly rougher, and part of the morphology becomes spherical. The characteristic peaks of different nanoparticles were determined by FTIR spectroscopy. The absorption peak at 422 cm^{-1} is attributed to the Zn-N stretching vibrational peak of ZIF-8, which is a bond formed by the coordination of Zn^{2+}

and 2- methylimidazole. ZIF-8 has characteristic peaks at 3135, 2926 and 1580 cm^{-1} due to stretching vibrations of aromatic C-H bonds, aliphatic CH bonds and C-N in 2-methylimidazole [37]. The new characteristic peak at 3415 cm^{-1} confirms the successful encapsulation of BA in ZIF-8 due to the presence of a large number of hydroxyl groups in BA. The methyl or methylene groups of GOx exhibit characteristic peaks at 2870 cm^{-1} and 2970 cm^{-1}, respectively [38] (Fig. 1D). These results indicated that BA/GOx@ZIF-8 nanoparticles were successfully prepared. The crystal structure of nanocomposites was determined using XRD technology. The XRD showed that ZIF-8, BA@ZIF-8, and BA/GOx@ZIF-8 nanoparticles all had six similar sharp diffraction peaks. The diffraction peaks at 7.26, 10.26, 12.68, 14.6, 16.38 and 17.92° were corresponded to the (101), (102), (103), (006), and (110) planes, respectively [39], indicating that the loading of BA and GOx did not destroy the crystal structure integrity of ZIF-8(Fig. 1E). Due to the negative charge of BA and GOx containing phenolic hydroxyl and carboxyl groups, the positive charge of ZIF-8 is neutralized after drug loading modification, resulting in a significant decrease in its positivity rate (Fig. 1H).

The porous internal structure of hydrogel can simulate the natural ECM, and promote cell adhesion, migration, and ECM deposition, making it an important candidate for accelerating wound healing [40]. In addition, injectable hydrogels are more suitable for wounds with different shapes to meet clinical needs. We have developed injectable photo crosslinked nanocomposite hydrogel. Firstly, we prepared GelMA by reacting gelatin and MA, the chemical structures of gelatin and GelMA were analyzed by ^{1}H NMR. We found a large number of amino acids and peptides in both gelatin and GelMA from the complex ^{1}H NMR spectra. It is worth noting that the appearance of methyl ($\delta = 1.9$ppm) and vinyl proton ($\delta = 5.4/5.7$ppm) signals, as well as the decrease in lysine signal intensity ($\delta = 2.99$ppm), demonstrate that gelatin has been successfully modified by MA to synthesize GelMA (Fig. 1F). Compared with sodium alginate and hyaluronic acid, GelMA retains the RGD sequence of gelatin, which can directly promote cell adhesion, proliferation, and differentiation without additional functionalization modifications; it can be specifically degraded by matrix metalloproteinases (MMPs); GelMA is easily composable with nanoparticles, which endows the hydrogel with a variety of functionalities; and its tunability meets the mechanical needs of different tissue repairs.

Subsequently, nanocomposite hydrogels were prepared by doping nanoparticles in GelMA (Z@Gel, BZ@Gel, and BGZ@GelMA). The injectability of the nanocomposite hydrogel was confirmed by extrusion experiments (Fig. 1I). After adding the photoinitiator LAP to the GelMA precursor solution, a jelly-like gel was formed by rapid cross-linking under 405 nm visible light irradiation. The microstructures of lyophilized nanocomposites hydrogels were observed by SEM. The microstructure of pure hydrogel and composite hydrogel doped with nanoparticles are basically the same, and both have 3D porous network structure, which provides the best environment for cell migration, gas exchange and nutrient transport (Fig. 1G).

Cytocompatibility evaluation of the nanocomposite hydrogels

Cytocompatibility is the basis for the in vivo application of nanocomposite hydrogels [11, 12]. We used L929 and HUVECs cells for cytocompatibility evaluation. The functional characteristics of HUVECs, such as surface receptors and signaling pathways, are highly similar to those of adult endothelial cells, and the experimental results have higher clinical reference value. Secondly, HUVECs are commonly used to assess cell migration (simulating wound closure), proliferation (tissue regeneration), and tubular structure formation (in vitro angiogenesis modeling), which can directly reflect the healing potential of the materials, and these characteristics make them ideal for studying the material or drug ideal cells for studying the ability of materials or drugs to promote angiogenesis. We evaluated the effects of hydrogel loaded with different concentrations of ZIF-8, BA@ZIF-8, and BA/GOx@ZIF-8 on the viability of HUVECs. The HUVECs were co-cultured with different concentrations of nanocomposite hydrogels for 24 h. The results showed that there was no effect on cell viability when the concentrations of ZIF-8 and BA@ZIF-8 reached 200 μg/mL, whereas when the concentration of BA/GOx@ZIF-8 reached more than 40 μg/mL caused a significant decrease in cell viability, which provided a concentration reference for our subsequent studies (Fig. S1).

We evaluated the effects of different nanocomposite hydrogels on the proliferation of HUVECs and L929 cells in a high-glucose inflammatory environment using CCK-8 assays. The results (Fig. 2A-B) showed that the viability of the two cells was significantly reduced under the high glucose inflammatory environment. When different nanocomposite hydrogels were added, all the cells showed sustained proliferation with the prolongation of the incubation time, suggesting that these nanocomposite hydrogels might be beneficial to the proliferation of the cells. We further selected L929 and HUVECs cells cultured for 3 days for live-dead staining, and the results showed that under high glucose inflammatory conditions, the number of both types of cells significantly decreased, while the cell viability was good after co-culture with Z@GelMA, BZ@GelMA and BGZ@GelMA hydrogel, and the number of cells in the BGZ@GelMA group significantly increased. The L929 and HUVECs

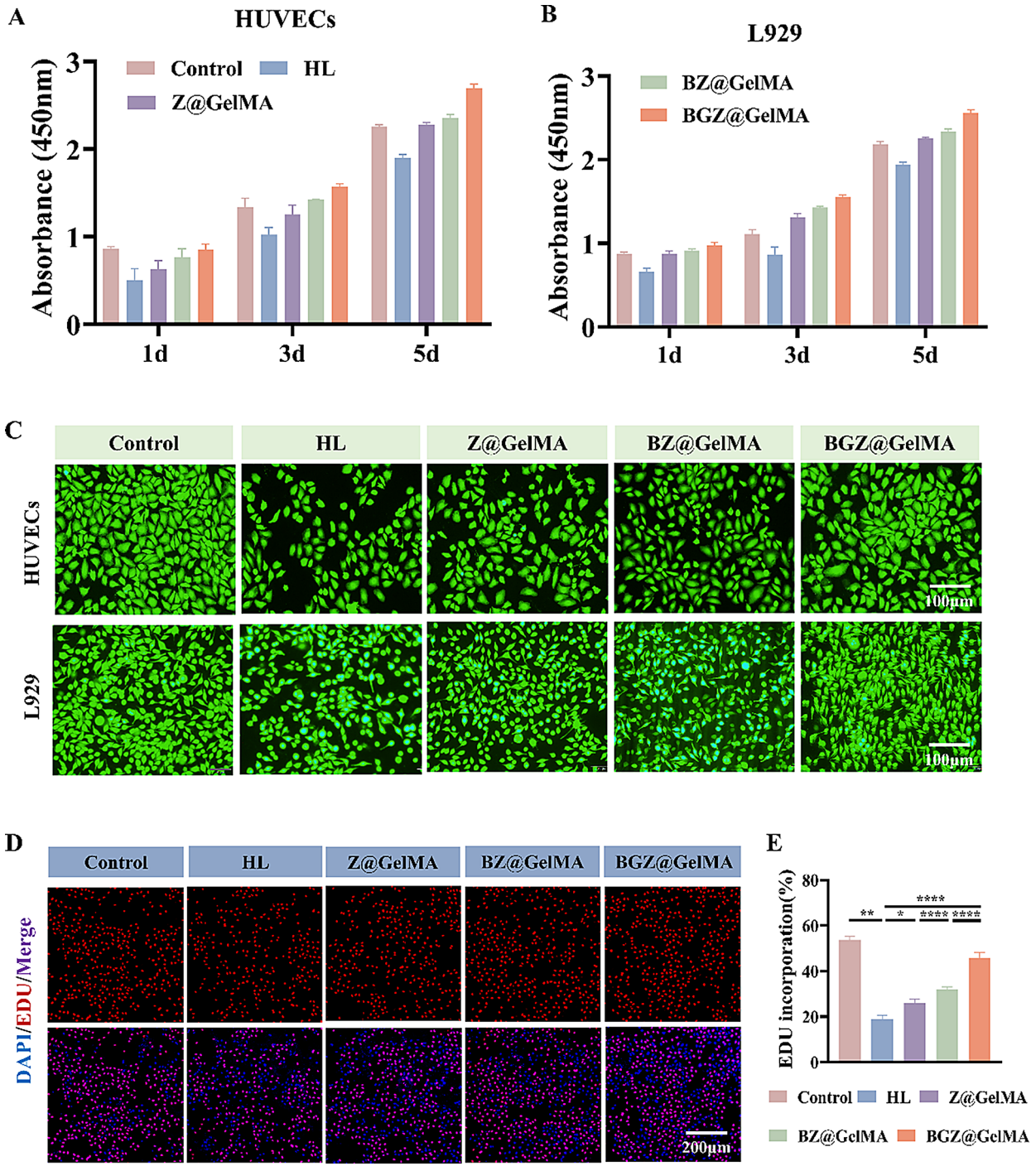

Fig. 2 Biocompatibility evaluation of BGZ@GelMA hydrogel. (**A**) Proliferation ability of HUVECs determined by the CCK-8 assay after different treatments. (**B**) Proliferation ability of L929 determined by the CCK-8 assay after different treatments. (**C**) Representative live/dead staining of HUVECs after incubation for 3 days (scale bar: 100 μm). (**D**) The representative images of the EDU assay (scale bar: 200 μm). (**E**) Quantification of the EDU assay

cells are alive (green) in different nanocomposite hydrogels, and there are almost no dead cells (red) (Fig. 2C). Cell flow was further confirmed the apoptosis rate of HUVECs cells increases significantly after being induced with HL, which could be alleviated by treating with Z@GelMA, BZ@GelMA, and BGZ@GelMA hydrogels. In comparison, BGZ@GelMA hydrogels have the most pronounced effect (Fig. S2).

The newly replicated DNA was labeled with EDU to accurately determine cell proliferation. We used EDU staining to evaluate the effect of hydrogel on HUVECs proliferation. The results showed that the BGZ@GelMA

group had the highest percentage of EDU-positive cells, which could significantly promote the proliferation of HUVECs (Fig. 2D). However, there were very few newly proliferating cells in the HL groups compared to the control group. The percentage of EDU-labeled cells indicated a consistent trend (Fig. 2E). Furthermore, reduced expression of Ki-67 was observed in HL-induced HUVECs, which was reversed by treatment with the BGZ@GelMA hydrogel (Fig. S3). Collectively, these findings suggested that BGZ@GelMA hydrogel improves the high-glycemic inflammatory microenvironment, provides a suitable environment for cell survival, and exhibits good cytocompatibility.

In addition, based on the results of the hemolysis test, we observed that the different nanocomposite hydrogels did not cause a significant hemolytic reaction, with a hemolysis rate of around 0.7% (Fig. S4).

Antibacterial activities of the nanocomposite hydrogels

The high-sugar environment provides sufficient nutrients for bacterial growth and accelerates bacterial proliferation, so continued bacterial infection is also an important factor in the difficulty of healing diabetic wounds [15]. *S. aureus* is widely present on the surface of the skin and is one of the most common pathogens causing skin infections. In addition, the proportion of *E. coli* causing wound infections is gradually increasing. We used a bacterial colony counting test to determine whether the BGZ@GelMA hydrogel could exert an antimicrobial effect. As shown in Fig. 3A, photographs of agar plates show a significant reduction in the number of colonies after *S. aureus* and *E. coli* co-culture with different hydrogels. The inhibition of *S. aureus* and *E. coli* co-cultured with BGZ@GelMA hydrogel was close to 100% (*S. aureus* was 95.3% and *E. coli* was 97.6%), indicating that this hydrogel has a wide range of antimicrobial properties. In contrast, the control group showed almost no antimicrobial effect, whereas Z@GelMA and BZ@GelMA exhibited moderate antimicrobial activity (Fig. 3B-C). We also analyzed the bacterial viability, and the results are shown that the control group exhibited limited inhibitory effects, while the bacterial viability of *S. aureus* and *E. coli* in the BGZ@GelMA group decreased significantly (Fig. S5). Similarly, the live/dead bacterial staining results indicated that virtually the majority bacteria remained viable in the control group (in green). The Z@GelMA group exhibited a partial antimicrobial effect due to Zn^{2+} activity. In contrast, the BZ@GelMA group exhibited significantly enhanced antibacterial activity due to the addition of BA. Notably, BGZ@GelMA hydrogel induced extensive bacterial death when co-cultured with *S. aureus* and *E. coli* (in red) (Fig. 3E). The same trend was observed for the quantitative ratios corresponding to live and dead bacteria (Fig. S6A-B). Finally, the microstructure of the bacterial membrane after different hydrogel treatments was examined by SEM to explore the antibacterial mechanism of the hydrogel. SEM images showed that *S. aureus* and *E. coli* in the control group were regular-shaped spherical and rod-shaped, respectively, with intact and smooth bacterial membrane structures. After co-incubation with BGZ@GelMA hydrogel bacteria, the physiological structure of the *S. aureus* and *E. coli* was disrupted, exhibiting varying degrees of contraction and rupture with leakage of contents, indicating a compromised cellular state. We used pseudo-colors to highlight the obviously damaged bacteria (Fig. 3D).

To explore the antibiofilm activity of BGZ@GelMA hydrogel in vitro, crystal violet staining assay and biomass quantitation were performed, and the biofilm in the group treated with BGZ@GelMA hydrogel remained barely viable, validating the significant antibiofilm activity (Fig. S7).

The flow cytometry results showed that after 4 h of intervention with different hydrogels BGZ@GelMA, the positive rates of PI uptake in *S. aureus* and *E. coli* were 33.8% and 33.6%, respectively, indicating that Zn^{2+} and BA can damage bacterial cell membranes (Fig. S8). Bacterial plate counting experiment confirm that ZIF-8@BA composite materials have stronger antibacterial ability than ZIF-8 or BA alone, $Zn^{2+}$and BA can synergistically exert antibacterial effects (Fig. S9).

In summary, the antimicrobial mechanism of BGZ@GelMA may be attributed to the following reasons: (1) The sustained release of Zn^{2+} ions disrupts the cell membrane of the bacteria [41]. (2) BA affects bacterial membrane permeability and influences bacterial biosynthesis and metabolism by inhibiting enzyme activity in the bacterium, thus realizing antibacterial effects [42]. (3) Natural polyphenols rich in phenolic hydroxyl groups can chelate metal ions and immobilize them on a substrate, enhancing the antimicrobial efficacy of the material [43]. These results demonstrated the potential of BGZ@GelMA hydrogel to prevent bacterial infection.

Protecting cell and mitochondrial function, scavenge ROS in vitro

Mitochondria are the primary site of cellular energy production and aerobic respiration, and the main source of intracellular ROS. In a hyperglycemic environment, ROS produced by mitochondria in endothelial cells accumulates and leads to the release of inflammatory factors, excessive oxidative stress causes mitochondrial dysfunction and affects cellular energy metabolism, which makes diabetic wounds difficult to heal [44, 45]. To evaluate the effects of different hydrogel treatments on intracellular ROS levels, we used DCFH-DA and Mito-SOX probes to quantify fluorescence intensity targeting ROS in the cytoplasm and mitochondria, and we used Mito-Tracker

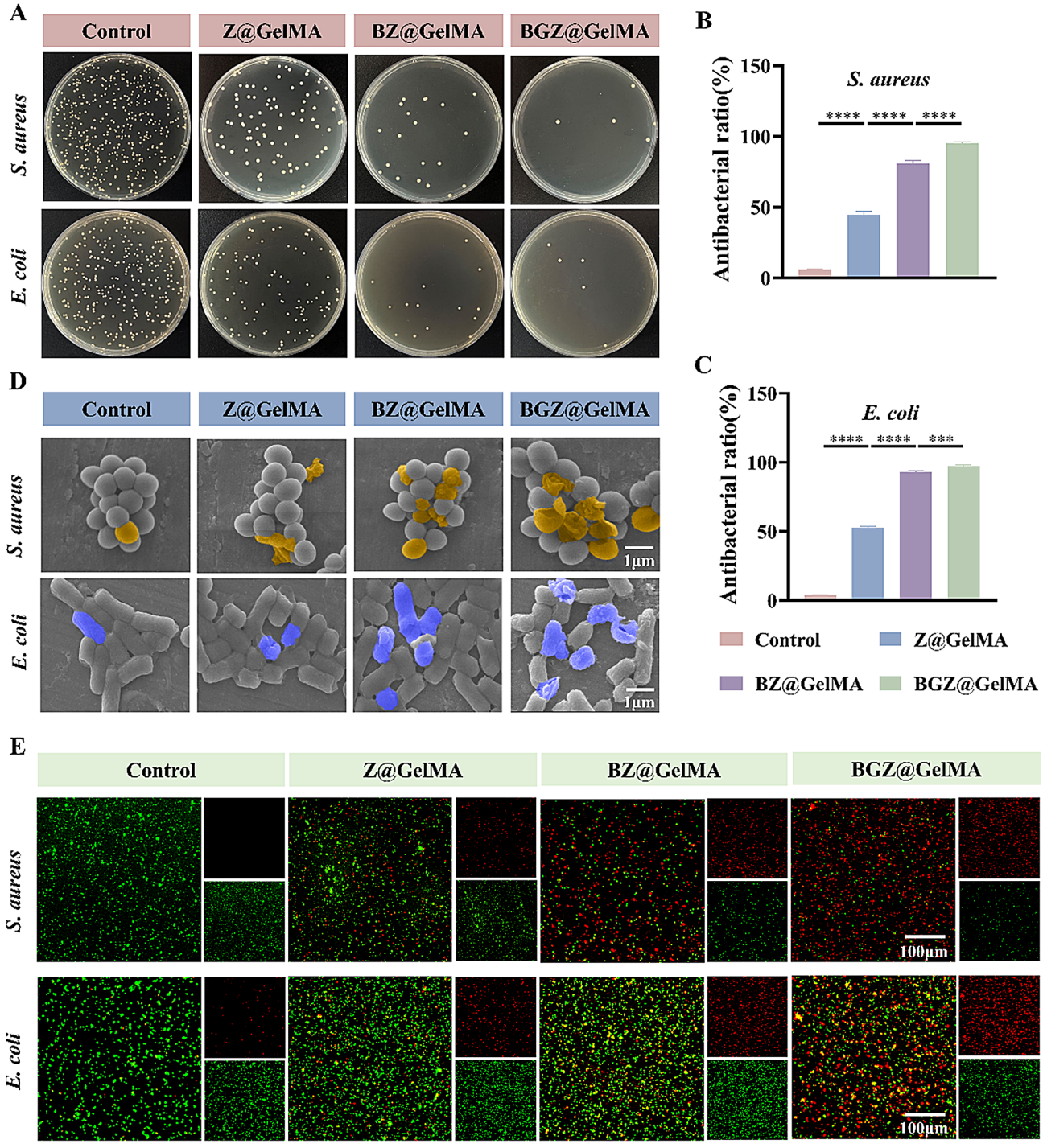

Fig. 3 The antimicrobial effect of BGZ@GelMA hydrogels in vitro. (**A**) Colonies of different groups of *S. aureus* and *E. coli* on agar plates. (**B**) Antimicrobial ratio of hydrogels against *S. aureus*. (**C**) Antimicrobial ratio of hydrogels against *E. coli*. (**D**) Representative SEM images of *S. aureus* and *E. coli* in different groups (scale bar: 1 μm). (**E**) Representative images of live/dead fluorescence staining of the *S. aureus* and *E. coli* (scale bar: 100 μm)

to specifically label intracellular mitochondria. After a 24 h incubation period, the fluorescence signal in Fig. 4A shows that the persistent hyperglycemic inflammatory microenvironment (HL group) stimulates the cells to produce excessive ROS. In contrast, the fluorescence intensity of all hydrogel groups decreased significantly, and that in BGZ@GelMA group was the lowest (Fig. 4D). Similarly, as shown in Fig. 4B, the persistent hyperglycemic environment strongly induced the accumulation of mtROS, whereas Z@GelMA and BZ@GelMA hydrogels significantly mitigated, the lowest red fluorescence was observed in the BGZ@GelMA group, suggesting

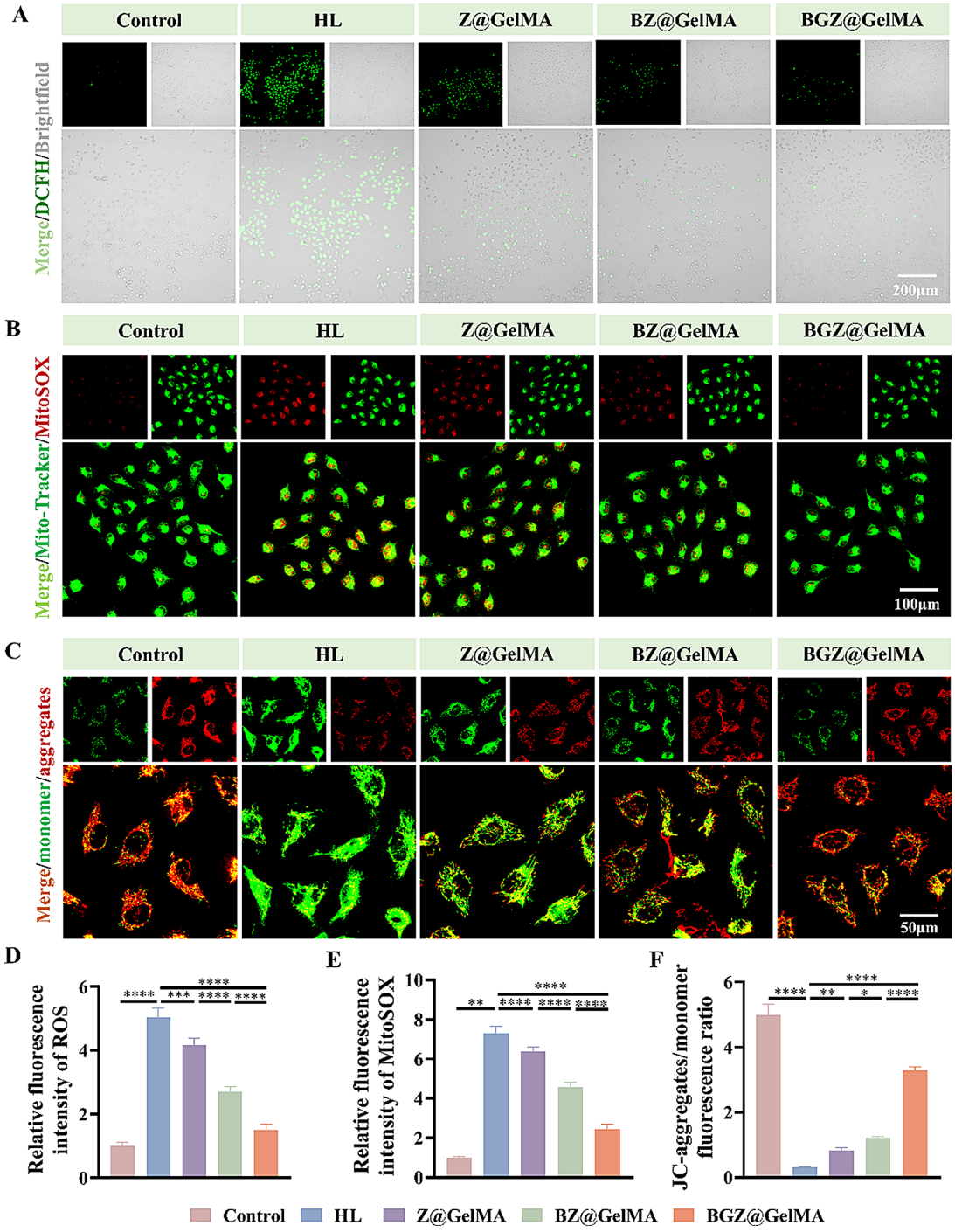

Fig. 4 Effect of BGZ@GelMA on intracellular ROS and mitochondrial function. (**A**) Representative Fluorescence images of intracellular ROS (scale bar: 200 μm). (**B**) Representative Fluorescence images of Mitochondrial ROS (scale bar: 100 μm). (**C**) Fluorescence images of mitochondrial membrane potential JC-1 staining (scale bar: 50 μm). Quantitative analysis of the (**D**) intracellular ROS, (**E**) mitochondrial ROS, and (**F**) JC-aggregates/monomer fluorescence ratio

good mtROS elimination, which was supported by the corresponding quantification of fluorescence intensity (Fig. 4E). Accumulation of ROS in mitochondria contributes to the abnormal opening of the mitochondrial permeability transition pore (mPTP), leading to disruption of the electrochemical potential (ΔΨm) across the inner mitochondrial membrane [46]. This disruption leads to mitochondrial matrix osmotic imbalance and disturbances in calcium metabolism. These changes ultimately lead to altered mitochondrial morphology and impaired

function, affecting cellular energy metabolism and ultimately apoptosis. Under normal conditions, the mitochondrial membrane potential is high and the JC-1 dye forms aggregates and emits red fluorescence. In contrast, when the membrane potential is abnormally low, the dye forms monomers and emits green fluorescence, indicating a change in mitochondrial membrane permeability. In Fig. 4C, we observed that the red fluorescent signals were significantly weakened or even disappeared in the HL group, indicating that the mitochondrial membrane potential was significantly reduced in the hyperglycemia inflammatory environment. The addition of Z@GelMA and BZ@GelMA slightly enhanced the red fluorescent signals intensity, however, The BGZ@GelMA group showed the most significant increase in fluorescence signal, indicating that BGZ@GelMA hydrogel can reduce the depolarization of mitochondrial membrane potential in hyperglycemia environment, and maintain the polarization of mitochondrial membrane potential at a normal level. The JC-aggregates/monomer fluorescence ratio also confirmed the same results (Fig. 4F). The above research results confirm that even in a sustained hyperglycemic inflammatory microenvironment, BGZ@GelMA nanocomposite hydrogel can also eliminate mtROS, protect mitochondrial function, and maintain cell energy metabolism.

Promoting cell migration and tube formation

Hyperglycemia-induced angiogenic dysfunction is one of the key factors contributing to the difficulty in healing diabetic wounds. Considering the key role of fibroblasts and endothelial cells in wound repair, the effect of BGZ@GelMA hydrogels on cell migration was evaluated. The Transwells assay results showed that the HL environment significantly inhibited the migration of L929 and HUVECs., HUVECs and L929 cells co-cultured with hydrogel extracts revealed a significantly faster migratory rate at 24 h compared with the HL group (Fig. 5A, S10A). Notably, the BGZ@GelMA group showed a superior ability to promote cell migration (Fig. 5D). The scratch assay is another experimental method for evaluating cell migration. As shown in Fig. 5B, S10B, in the HL environment, HUVECs and L929 cells treated with hydrogel extracts migrated rapidly and the scratch area was significantly reduced after 24 h of culture. The migration rate of HUVECs cultured with Z@GelMA, BZ@GelMA and BGZ@GelMA extracts were 36.21%, 42.17%, and 52.19%, respectively, which was higher than 30% of the HL group (Fig. 5E). The results showed that the nanocomposite hydrogels significantly promoted the cell migration of L929 and HUVECs, while Zn^{2+}, BA and GOx all acted synergistically.

Endothelial cells are the main cells involved in the process of neovascularization during wound healing. Therefore, we analyzed the tube formation of HUVECs on the BGZ@GelMA hydrogels. The observed photographs in Fig. 5C showed that HUVEC in the BG@GelMA and BGZ@GelMA groups showed an increase in cellular lattices and nodes, and the cells became denser and were able to form good tubular and mesh structures under a hyperglycemic inflammatory environment, which were hardly visible in the HL group. Quantitative analysis showed significant improvement in the number of tube junctions in the BG@GelMA and BGZ@GelMA groups (Fig. 5F).

During wound healing, angiogenesis is closely related to growth factors such as VEGF and CD31 secreted by vascular endothelial cells [47]. It has been shown that Zn^{2+} and BA can promote angiogenesis by upregulating the expression of VEGF [48, 49]. The expression levels of VEGF in HUVECs were evaluated by different methods after treating with different hydrogels for 24 h in a high-glucose inflammatory environment. Immunofluorescence imaging revealed significantly elevated VEGF levels in the BZ@GelMA group and BGZ@GelMA group compared to the HL group (Fig. 6A). Quantitative analysis shows the higher relative fluorescence intensity of the BGZ@GelMA group (Fig. 6D). CD31 immunofluorescence staining and quantitative analysis also showed the same trends (Fig. S11). WB analysis further confirmed that VEGF expression was significantly upregulated in the BGZ@GelMA group (Fig. 6B-C). These results indicate that the BGZ@GelMA hydrogel substantially boosts angiogenic factor expression and fosters neovascularization, potentially aiding in vascular regeneration and endothelial repair in chronic wounds. The above results indicated that BGZ@GelMA hydrogel is expected to accelerate diabetic wound healing by promoting the proliferation and migration of endothelial cells, up-regulating the expression of VEGF and CD31 to promote blood vessel formation.

AGEs are also the key factors leading to delayed healing in diabetes. The AGEs activate downstream signaling pathways (e.g., NF-κB) by binding to cell-surface receptors (RAGEs), resulting in increased secretion of the cytokines IL-6, IL-1β, and TNF-α secretion to increase, triggering inflammatory responses and oxidative stress [50]. In addition, AGEs inhibit endothelial cell proliferation and migration, leading to delayed diabetic wound healing [51]. Therefore, anti-glycosylation may help to improve the diabetic wound environment. In this study, we further used AGEs to interfere with HUVECs, to detect the expression of inflammatory factors, cell proliferation and migration and to observe the anti-AGEs effect of different hydrogels. The experimental results indicate that the expression of inflammatory factors was significantly increased under AGEs stimulation, and cell migration was inhibited, the Z@GelMA, BZ@GelMA

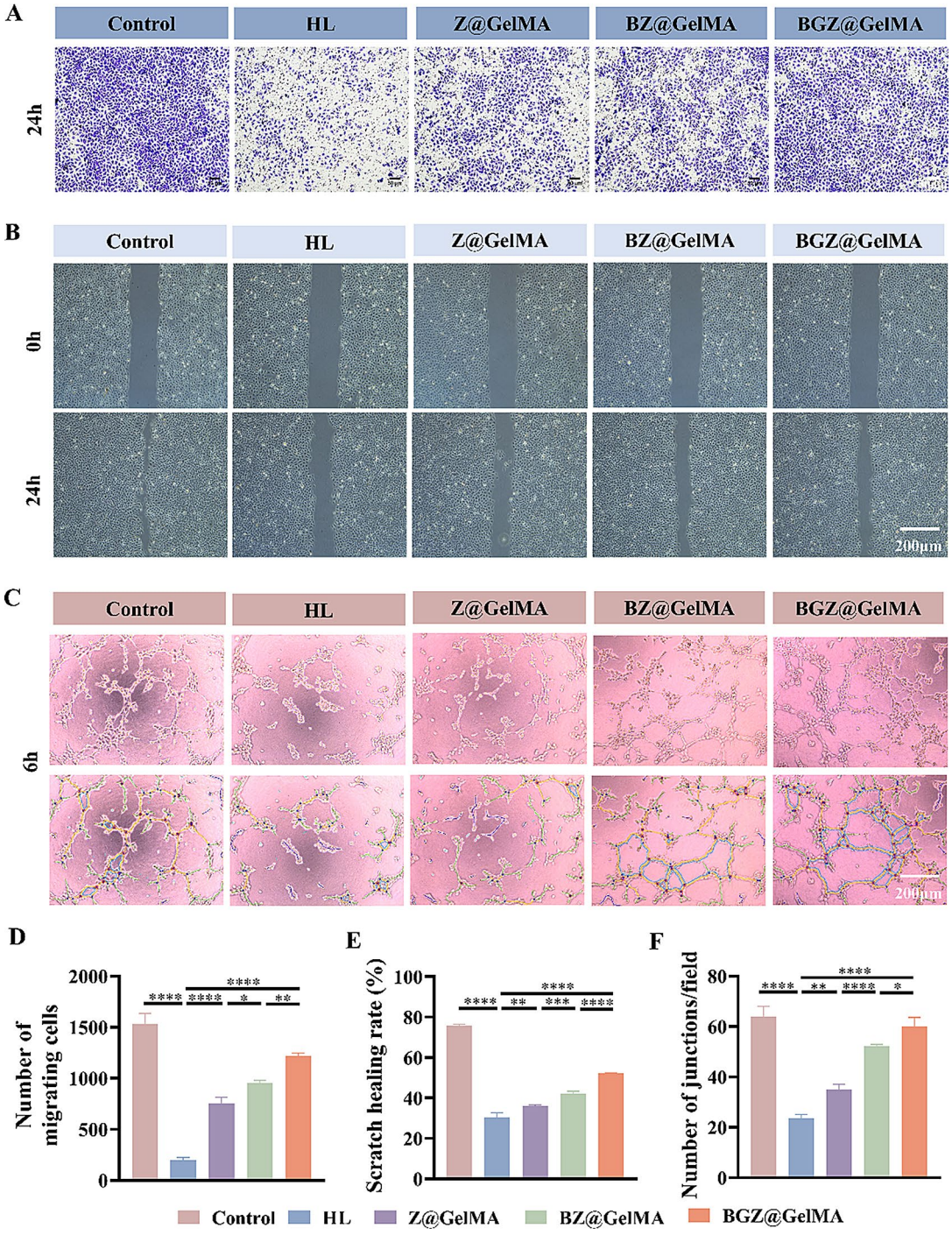

Fig. 5 BGZ@GelMA promotes cell migration and angiogenesis in vitro. (**A**) The representative images of the transwell assay (scale bar: 50 μm). (**B**) The representative images of scratch migration assay (scale bar: 200 μm). (**C**) Representative images of tube formation experiments (scale bar: 200 μm). (**D**) Quantitative analysis of HUVECs transwell migration cells counts. (**E**) Quantitative analysis of the scratch healing rate of HUVECs. (**F**) Quantitative analysis of the number of junctions

and BGZ@GelMA hydrogel extract can reverse this phenomenon, and BGZ@GelMA hydrogel can significantly reduce the expression of inflammatory factors (Fig. S12A-C) and promote cell migration (Fig. S12D-G).

Promoting wound healing mechanism in vitro

To further explore the regulatory mechanism of the BGZ@GelMA hydrogel regulating HUVECs. We determined the mRNA profile of HUVECs treated with BGZ@GelMA using RNA-Seq analysis. As shown in Fig. 7A,

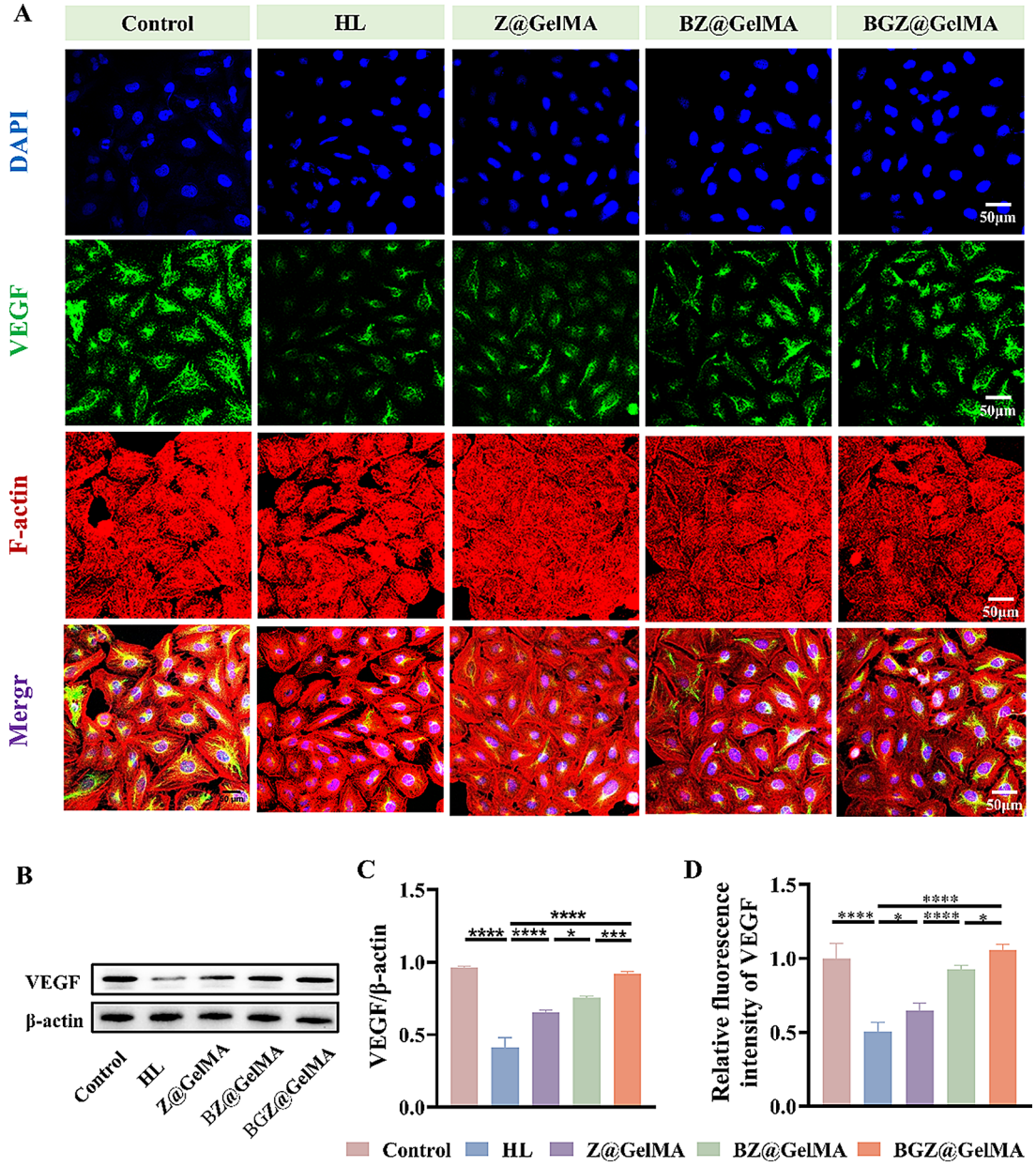

Fig. 6 BGZ@GelMA hydrogel promotes VEGF expression. (**A**) Immunofluorescence images of VEGF in different treatment groups, F-actin (red), VEGF(green), DAPI(blue) (scale bar: 50 μm). (**B**) The protein expression of VEGF in the different groups. (**C**) Quantitative analysis of VEGF protein. (**D**) Quantitative analysis relative fluorescence intensity of VEGF

principal component analysis (PCA) shows that the samples in each group are independently clustered. The volcano map in Fig. 7B shows that there are 235 differentially expressed genes (DEGs), including 70 upregulated genes and 165 downregulated genes between the two groups. We conducted Gene Ontology (GO) enrichment analysis, including categories of biological processes (BP), molecular functions (MF), and cellular components (CC) to analyze these DEGs. It focuses on epidermal tissue development, keratinocyte differentiation, endothelial cell proliferation, immune defense response, and metabolism-related enzymes, which are closely related to the whole process of wound healing (Fig. 7C). The Kyoto Encyclopedia of Genes and Genomes (KEGG) enrichment analysis was then applied to analyze potential signaling pathways, and furthermore showed changes in the expression of specific genes in a complex clustering diagram (Fig. 7D). The KEGG enrichment analysis shows BGZ@GelMA regulated the peroxisome proliferator-activated receptor (PPAR) signaling pathway and some metabolic pathways in endothelial cells. The expression of specific genes was shown in the clustered string

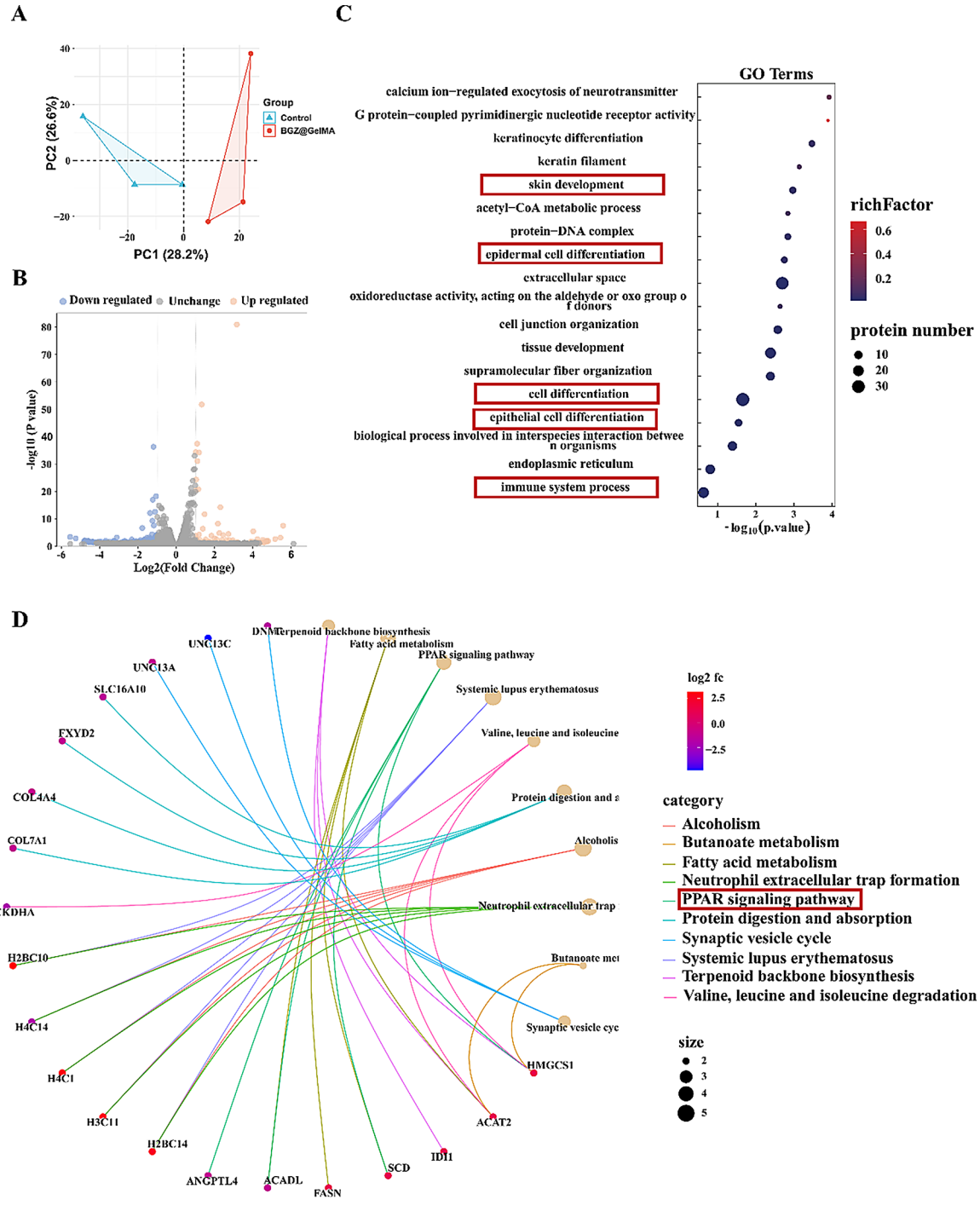

Fig. 7 Regulatory mechanism of BGZ@GelMA in promoting diabetic wound healing. (**A**) PCA analysis of the global sample. (**B**) Volcano plot displaying up-regulated and down-regulated genes (fold change ≥ 2 and $p < 0.05$) in HUVECs co-cultured with BGZ@GelMA. (**C**) Differentially expressed terms analyzed by the GO enrichment method. (**D**) Analysis of KEGG-enriched signaling pathways of DEGs and the corresponding genes

plot, such as COL7A1 and COL4A4, involved in collagen formation, while ACADL, BCKDHA, and HMGCS1 were involved in mitochondrial metabolism. According to reports, the PPAR family and signaling pathways are involved in multiple stages of skin repair after injury [52]. PPAR consists of three subtypes, PPAR -αmainly participates in the oxidative metabolism of fatty acids, provides sufficient energy for endothelial cells, and participates in early inflammatory repair of the skin [53]. PPARβ/δ is primarily involved in cell growth and differentiation and regulates mitochondrial function and metabolism and promotes proliferation and adhesion

of keratinocytes [54]. PPARγ is widely involved in lipid metabolism and plays an important role in inflammatory response, immune regulation, cell proliferation, and survival [35]. PPARγ is an upstream signaling molecule of NF-κB. Activated PPARγ can inhibit the activation of NF-κB transcription factors, thus suppressing the inflammatory response [55, 56]. These results suggest that BGZ@Gel hydrogel may be involved in the healing process of diabetic wounds by promoting keratinized fiber formation, endothelial cell proliferation, mitochondrial metabolism, activation of the PPAR pathway, and immunomodulation. BA may affect metabolism and inflammatory response by directly or indirectly regulating the expression and activity of PPARs (PPARα, PPARγ). Some studies have shown that baicalein is able to inhibit mitochondrial function and kinetic changes, exert mitochondrial protective and antioxidant effects, and inhibit apoptosis through the upregulation of PPARγ coactivator 1α, Nrf2, and related redox signaling pathways [57]. Baicalein exerts beneficial effects on macrophage lipid accumulation and inflammatory responses through activation of the PPARγ/liver X receptor α (LXRα) signaling pathway [58].

Diabetic wounds healing in vivo

Combined with BGZ@GelMA nanocomposite hydrogel has good antibacterial, pro-angiogenic, and mitochondrial homeostasis restoration effects in vitro. We further verified the in vivo therapeutic effect through a diabetic rat wound model. Diabetic SD rats were equally divided into three groups, blank control group without any treatment, GelMA hydrogel dressing, and BGZ@GelMA hydrogel dressing. The schematic illustration is shown in Fig. 8A. In all groups, the BGZ@GelMA hydrogel represents a faster wound healing process, in which, on the 21st day, the BGZ@GelMA group observed good wound healing ability and a wound healing rate of 98.5%, which was superior to other groups (Fig. 8B-D). After that, we performed a comprehensive histological analysis to assess the change in wound length, wound healing rate, and skin morphology. H&E staining analysis showed that in the BGZ@GelMA hydrogel group, the inflammatory cell infiltration level was significantly reduced on the 7th day, and after 21 days of BGZ@GelMA hydrogel treatment, epithelial metaplasia has typical skin layer structure and morphological feature (Fig. 8E). In addition, we have found that after 7 days of BGZ@GelMA hydrogel treatment, the length of the wound gape was significantly reduced compared to the other groups (Fig. 8F). Subsequently, Masson staining was used to evaluate the collagen deposition in each group. After 21 days of BGZ@GelMA hydrogel treatment, a large amount of well-structured collagen and skin appendages were observed in the subepidermal tissue of the wound compared to the GelMA hydrogel group and the control group. (Figures 8G and 9A). We found that the hydrogel-only group also had some collagen fiber deposition, which can be attributed to the fact that GelMA hydrogels contain the common Arg-Gly-Asp (RGD) fraction, a tripeptide that promotes cell proliferation, differentiation, and adhesion [59]. The results indicated that BGZ@GelMA hydrogel significantly promoted the formation and maturation of granulation tissue and accelerated collagen deposition in diabetic wounds.

Due to the complex physiological process of wound healing, it can be roughly divided into three stages: inflammation, proliferation, and recovery. These three stages appear to be independent yet interconnected. To explore the therapeutic effects of BGZ@GelMA hydrogel in vivo in the inflammatory stage, we evaluated the expression of pro-inflammatory cytokines at the wound site after 7 days of treatment using immunohistochemistry, as shown in Fig. 9B, the expression level of IL-6 and TNF-α was highest in the DM group on day 7, indicating a severe inflammatory response. Compared with the DM group and GelMA group, the levels of TNF-αand IL-6 in the BGZ@GelMA hydrogel group were significantly reduced (Fig. 9C-D). This indicates that the BGZ@GelMA sustained release of BA alleviates local inflammatory reactions and reduces the expression of pro-inflammatory cytokines. These results suggest that, the BGZ@GelMA hydrogel treatment can significantly alleviate the inflammatory reaction of chronic diabetes wounds.

Newly formed blood vessels actively contribute to the wound repair process by supplying nutrients and oxygen to growing tissues. VEGF can accelerate wound healing by stimulating angiogenesis, and vascular markers CD31 was performed to assess neovascularization. however, local VEGF production is often limited in diabetic wounds, resulting in delayed wound healing. Therefore, we evaluated angiogenesis in each group of wounds during the proliferation stage. On the 14st day, we performed immunohistochemical staining on VEGF and CD31 in the treated wound tissue, as shown in the Fig. 9E, the levels of VEGF and CD31 in the BGZ@GelMA hydrogel group were significantly higher than those in the blank control group and GelMA group, and a large number of new blood vessels can be seen at the wound. Quantitative analysis shows the same trend (Fig. 9F-G). This may be due to the adhesive of hydrogel and the synergistic effect of Zn^{2+} and BA to promote the proliferation and migration of endothelial cells, create a microenvironment conducive to angiogenesis, and thus induce angiogenesis. H&E staining showed no obvious damage to the heart, liver, spleen, lung, kidney and other major organs (Fig. S13). These results confirmed that BGZ@GelMA hydrogel has good biological safety and can accelerate the growth of diabetes wounds.

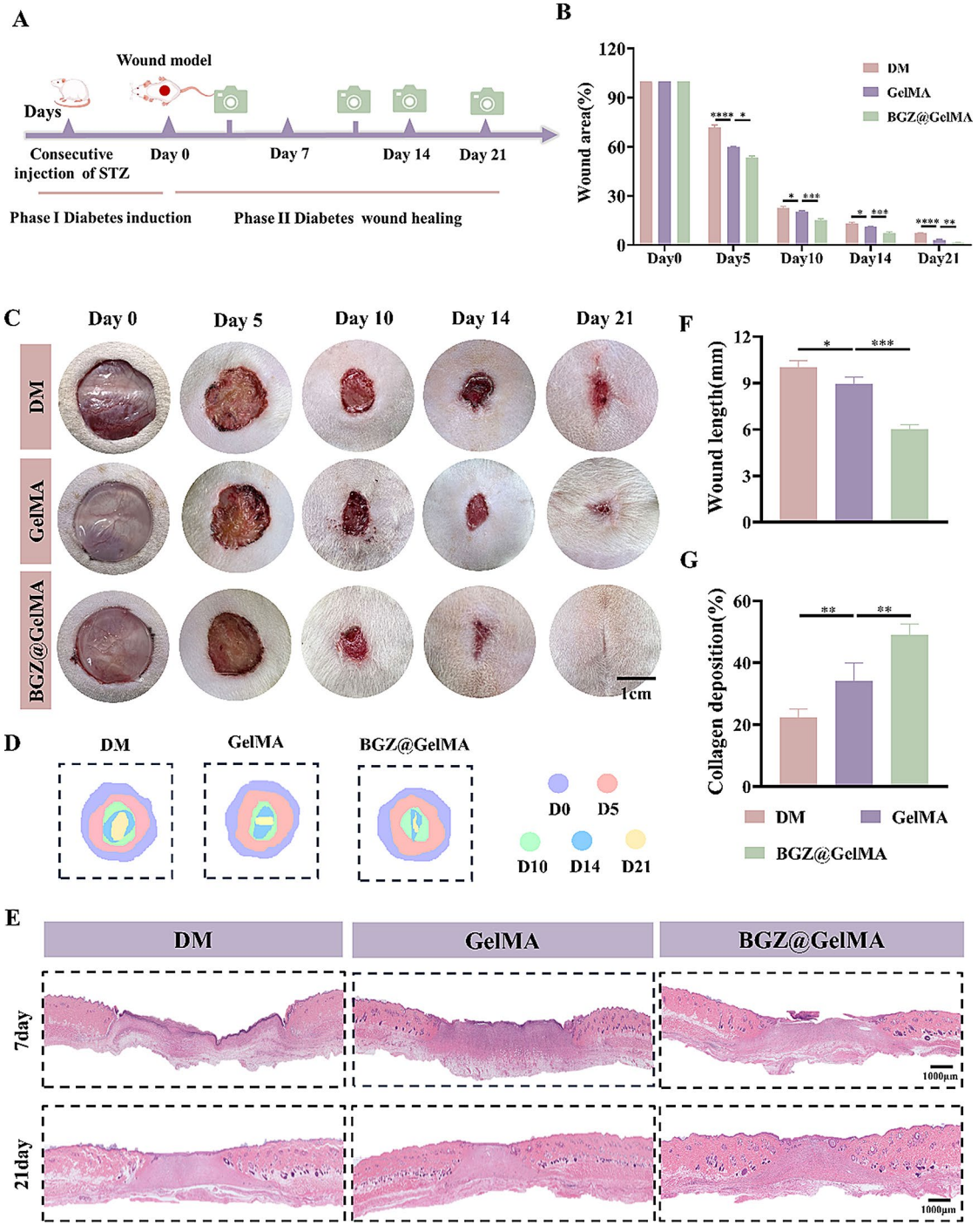

Fig. 8 BGZ@GelMA hydrogel promotes diabetic wound healing in vivo. (**A**) Schematic diagram of the wound treatment process in diabetic rats. (**B**) Percentage of trauma area in diabetic rats at different time points. (**C**) Representative digital photos showing the healing progression of diabetic wounds in rats subjected to various treatments (scar bar: 10 mm). (**D**) Images of diabetic wound traces on days 0, 5, 10, 14, and 21. (**E**) H&E staining of the collected wound skin tissue in different groups at 7d and 14d. (**F**) Quantitative analysis of the wound edge length in different groups. (**G**) Quantitative analysis of collagen deposition in different groups

So far, despite our success, our research still has some limitations. First of all, in terms of the synthesis of nanomaterials, we lacked in-depth research on different material concentrations, and did not systematically compare the injectable hydrogel concentration, crosslinking time and light intensity; Secondly, we designed to use GOx to reduce local blood glucose without considering its impact on systemic blood glucose. These provide direction and

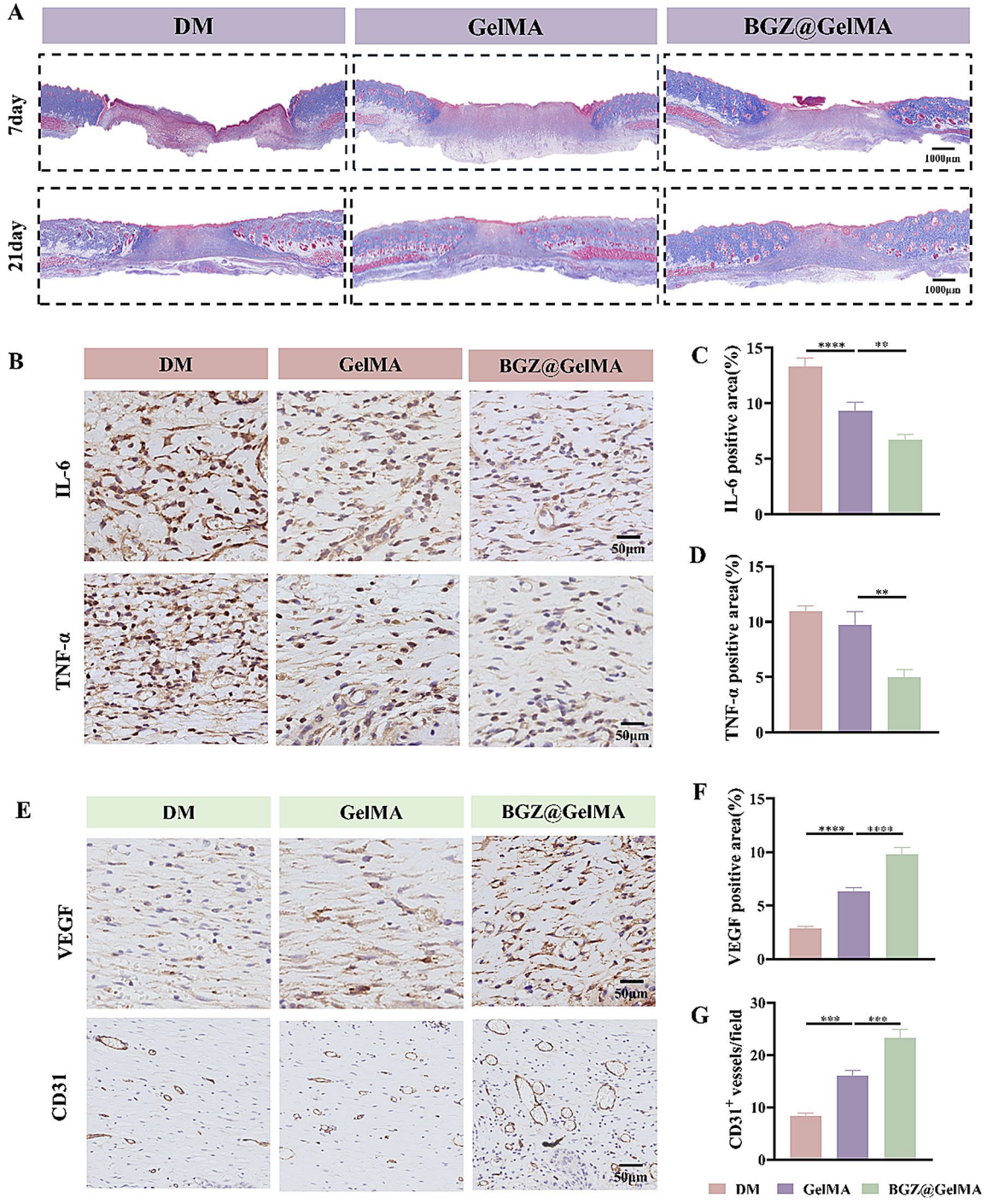

Fig. 9 The effect of the BGZ@GelMA hydrogel on the three wound healing stages. (**A**) Masson staining of the collected wound skin tissue in different groups at 7d and 14d. (**B**) Representative immunohistochemistry staining images of IL-6 and TNF-α in the different groups (scale bar: 50 μm). (**C**-**D**) Statistical analysis of the positive area (IL-6 and TNF-α). (**E**) Representative immunohistochemistry staining images of VEGF and CD31 in the different groups (scale bar: 50 μm). (**F**-**G**) Statistical analysis of the positive area (VEGF and CD31)

ideas for our future research, and are also worth further exploration in the future.

Conclusion

In this study, an injectable photo-crosslinked nanocomposite hydrogel (BGZ@GelMA) system composed of ZIF-8 loaded BA and GOx nanoparticles loaded into GelMA was developed, accelerating the healing of diabetic wounds. First of all, the injectability of GelMA can meet different forms of wounds, and the three-dimensional structure of GelMA facilitates gas exchange at the wound site and promotes cell adhesion. Second, BGZ@GelMA hydrogel remodels the diabetic wound microenvironment by lowering local glucose and pH levels. ZIF-8 decomposes and releases BA and Zn^{2+} in an acidic environment. Zn^{2+} and BA can synergistically exert antibacterial, anti-inflammatory, and angiogenic effects. It is important that BGZ@GelMA hydrogel can alleviate oxidative stress, clear ROS in cells and mitochondria, and restore mitochondrial membrane potential to maintain mitochondrial stability. Therefore, we designed BGZ@GelMA hydrogel focusing on the level of mitochondria provides a new idea for wound healing in diabetes.

Supplementary Information

The online version contains supplementary material available at https://doi.org/10.1186/s12951-025-03427-6.

Supplementary Material 1

Acknowledgements
Not applicable.

Author contributions
Danlei Qin: Writing–original draft, Software, Project administration, Methodology, Data curation, Conceptualization. Weiting Hu: Validation, Methodology, Data curation. Yanqin Guo: Investigation, Data curation, Funding acquisition. Rui Cheng: Methodology, Data curation, Funding acquisition. Fengxiang Hao: Project administration, Methodology, Formal analysis. Bin Zhao: Writing–review & editing, Investigation, Data curation, Conceptualization.

Funding
This work was supported by Basic Research Program of Shanxi Province (No. 202303021222335) (No. 202403021211121). Scientific and Technological Innovation Programs of Higher Education Institutions in Shanxi (STIP) (grant numbers 2023L086, 2022L145).

Data availability
No datasets were generated or analysed during the current study.

Declarations

Ethics approval and consent to participate
All animal experiments were approved by the Animal Protection and Ethics Committee of Shanxi Medical University, School of Stomatology.

Consent for publication
All authors consent for publication.

Competing interests
The authors declare no competing interests.

Author details
[1]Shanxi Medical University School and Hospital of Stomatology, Shanxi Province Key Laboratory of Oral Diseases Prevention and New Materials, Taiyuan, Shanxi 030001, China
[2]Department of Medical Imaging, Shanxi Medical University, Taiyuan, Shanxi 030001, China
[3]The Second Clinical Medical College, Shanxi Medical University, Taiyuan, Shanxi 030001, China
[4]Department of Ultrasound, The Second Hospital of Shanxi Medical University, 382 Wuyi Road, Taiyuan, Shanxi 030001, China
[5]Department of Endocrinology, The Second Hospital of Shanxi Medical University, 382 Wuyi Road, Taiyuan, Shanxi 030001, China

Received: 9 March 2025 / Accepted: 1 May 2025
Published online: 19 May 2025

References

1. Birkenfeld AL, Mohan V. Prediabetes remission for type 2 diabetes mellitus prevention. Nat Rev Endocrinol. 2024;20:441–2.
2. Boulton AJ, Vileikyte L, Ragnarson-Tennvall G, Apelqvist J. The global burden of diabetic foot disease. Lancet. 2005;366:1719–24.
3. Lin C, Hu Y, Lin Z, Du L, Hu Y, Ouyang L, Xie X, Cheng P, Liao J, Lu L, Zeng R, Xia P, Hou Z, Liu G, Hu H. MMP-9 responsive hydrogel promotes diabetic wound healing by suppressing ferroptosis of endothelial cells. Bioact Mater. 2025;43:240–54.
4. Shi M, Du Z, Qi Y, Li W, Hu H, Lin X, Wang S, Tang Z, Zhou M. Wound microenvironment-responsive glucose consumption and hydrogen peroxide generation synergistic with Azithromycin for diabetic wounds healing. Theranostics. 2022;12:2658–73.
5. Zhang W, Chen L, Xiong Y, Panayi AC, Abududilibaier A, Hu Y, Yu C, Zhou W, Sun Y, Liu M, Xue H, Hu L, Yan C, Xie X, Lin Z, Cao F, Mi B, Liu G. Antioxidant therapy and Antioxidant-Related bionanomaterials in diabetic wound healing. Front Bioeng Biotechnol. 2021;9:707479.
6. Xiong Y, Chu X, Yu T, Knoedler S, Schroeter A, Lu L, Zha K, Lin Z, Jiang D, Rinkevich Y, Panayi AC, Mi B, Liu G, Zhao Y. Reactive oxygen Species-Scavenging nanosystems in the treatment of diabetic wounds. Adv Healthc Mater. 2023;12:e2300779.
7. Sharma S, Schaper N, Rayman G, Microangiopathy. Is it relevant to wound healing in diabetic foot disease? Diabetes Metab Res Rev. 2020;36(Suppl 1):e3244.
8. Yang H, Lv D, Qu S, Xu H, Li S, Wang Z, Cao X, Rong Y, Li X, Wu H, Chen Y, Zhu J, Tang B, Hu Z. A ROS-Responsive lipid nanoparticles release multifunctional hydrogel based on microenvironment regulation promotes infected diabetic wound healing. Adv Sci (Weinh). 2024;11:e2403219.
9. Li Y-J, Wei S-C, Chu H-W, Jian H-J, Anand A, Nain A, Huang Y-F, Chang H-T, Huang C-C, Lai J-Y. Poly-quercetin-based NanoVelcro as a multifunctional wound dressing for effective treatment of chronic wound infections. Chem Eng J. 2022;437:135315.
10. Pu M, Cao H, Zhang H, Wang T, Li Y, Xiao S, Gu Z. ROS-responsive hydrogels: from design and additive manufacturing to biomedical applications. Mater Horiz. 2024;11:3721–46.
11. Lin H-Y, Wang S-W, Mao J-Y, Chang H-T, Harroun SG, Lin H-J, Huang C-C, Lai J-Y. Carbonized nanogels for simultaneous antibacterial and antioxidant treatment of bacterial keratitis. Chem Eng J. 2021;411:128469.
12. Luo L-J, Nguyen DD, Huang C-C, Lai J-Y. Therapeutic hydrogel sheets programmed with multistage drug delivery for effective treatment of corneal abrasion. Chem Eng J. 2022;429:132409.
13. Amirthalingam S, Rajendran AK, Moon YG, Hwang NS. Stimuli-responsive dynamic hydrogels: design, properties and tissue engineering applications. Mater Horiz. 2023;10:3325–50.
14. Fu LH, Qi C, Lin J, Huang P. Catalytic chemistry of glucose oxidase in cancer diagnosis and treatment. Chem Soc Rev. 2018;47:6454–72.
15. Li D, Chen T, Zhang Y, Xu Y, Niu H. Synergistical starvation and Chemo-Dynamic therapy for combating Multidrug-Resistant Bacteria and accelerating diabetic wound healing. Adv Healthc Mater. 2021;10:e2100716.
16. Tian M, Zhou L, Fan C, Wang L, Lin X, Wen Y, Su L, Dong H. Bimetal-organic framework/GOx-based hydrogel dressings with

antibacterial and inflammatory modulation for wound healing. Acta Biomater. 2023;158:252–65.
17. Liao Y, Zhang Z, Zhao Y, Zhang S, Zha K, Ouyang L, Hu W, Zhou W, Sun Y, Liu G. Glucose oxidase: an emerging multidimensional treatment option for diabetic wound healing. Bioact Mater. 2025;44:131–51.
18. Deng Y, Ouyang X, Sun J, Shi X, Li Y, Chan YK, Yang W, Peng S. Rapid sterilisation and diabetic cutaneous regeneration using cascade bio-heterojunctions through glucose oxidase-primed therapy. Bioact Mater. 2023;25:748–65.
19. Yang CJ, Nguyen DD, Lai JY. Poly(l-Histidine)-Mediated On-Demand therapeutic delivery of roughened ceria nanocages for treatment of chemical eye injury. Adv Sci (Weinh). 2023;10:e2302174.
20. Ger TY, Yang CJ, Bui HL, Lue SJ, Yao CH, Lai JY. Alginate-functionalized nanoceria as ion-responsive eye drop formulation to treat corneal abrasion. Carbohydr Polym. 2025;352:123164.
21. Ger T-Y, Yang C-J, Ghosh S, Lai J-Y. Biofunctionalization of nanoceria with sperminated hyaluronan enhances drug delivery performance for corneal alkali burn therapy. Chem Eng J. 2023;476:146864.
22. Palma FR, Gantner BN, Sakiyama MJ, Kayzuka C, Shukla S, Lacchini R, Cunniff B, Bonini MG. ROS production by mitochondria: function or dysfunction? Oncogene. 2024;43:295–303.
23. Tong Q, Yi Z, Ma L, Tan Y, Liu D, Cao X, Ma X, Li X. Microenvironment-Responsive antibacterial, Anti-Inflammatory, and antioxidant Pickering emulsion stabilized by Curcumin-Loaded tea polyphenol particles for accelerating infected wound healing. ACS Appl Mater Interfaces. 2024;16:44467–84.
24. Yang D, Zhao W, Zhang S, Liu Y, Teng J, Ma Y, Huang R, Wei H, Chen H, Zhang J, Chen J. Dual Self-Assembly of puerarin and silk fibroin into supramolecular nanofibrillar hydrogel for infected wound treatment. Adv Healthc Mater. 2024;13:e2400071.
25. Yi Y, Yang Z, Zhou C, Yang Y, Wu Y, Zhang Q. Quercetin-encapsulated GelMa hydrogel microneedle reduces oxidative stress and facilitates wound healing. Nano TransMed. 2024.
26. Song Y, Han N, Guo Z, Li H, Guo M, Dou M, Ye J, Peng Z, Lu X, Li M, Wang X, Bai J, Du S. Baicalein-modified Chitosan nanofiber membranes with antioxidant and antibacterial activities for chronic wound healing. Int J Biol Macromol. 2024;279:134902.
27. Liu Z, Xiang H, Deng Q, Fu W, Li Y, Yu Z, Qiu Y, Mei Z, Xu L. Baicalin and Baicalein attenuate hyperuricemic nephropathy via inhibiting PI3K/AKT/NF-κB signalling pathway. Nephrol (Carlton). 2023;28:315–27.
28. Yu Z, Li Q, Wang Y, Li P. A potent protective effect of Baicalein on liver injury by regulating mitochondria-related apoptosis. Apoptosis. 2020;25:412–25.
29. Yang J, Chen A, He X, Lu S. Fabrication of baicalein-encapsulated zeolitic imidazole framework as a novel nanocomposited wound closure material to persuade pH-responsive healing efficacy in post-caesarean section wound care. Int Wound J. 2023;20:1921–33.
30. Gong J, Wang H, Xie C, Dai Y, Wang Y, Guo W. A multifunctional injectable hydrogel for boosted diabetic wound healing assisted by Quercetin-ZIF system. Chem Eng J. 2024;495.
31. Yang J, Zeng W, Xu P, Fu X, Yu X, Chen L, Leng F, Yu C, Yang Z. Glucose-responsive multifunctional metal-organic drug-loaded hydrogel for diabetic wound healing. Acta Biomater. 2022;140:206–18.
32. Zhang C, Hong S, Liu MD, Yu WY, Zhang MK, Zhang L, Zeng X. Zhang X Z. pH-sensitive MOF integrated with glucose oxidase for glucose-responsive insulin delivery. J Control Release. 2020;320:159–67.
33. Li Y, Xu C, Mao J, Mao L, Li W, Liu Z, Shin A, Wu J, Hou L, Li D, Lin K, Liu J. ZIF-8-based nanoparticles for inflammation treatment and oxidative stress reduction in periodontitis. ACS Appl Mater Interfaces. 2024;16:36077–94.
34. Shao Y, Zhou X, Zhou S, Long J, Jin L, Shi X, Zhou L, Zhang Y, Fan D. Injectable DMM/GelMA hydrogel for diabetic wound healing via regulating mitochondrial metabolism and macrophage repolarization. Colloids Surf B Biointerfaces. 2025;248:114488.
35. Shu F, Huang H, Xiao S, Xia Z, Zheng Y. Netrin-1 co-cross-linked hydrogel accelerates diabetic wound healing in situ by modulating macrophage heterogeneity and promoting angiogenesis. Bioact Mater. 2024;39:302–16.
36. Lao A, Wu J, Li D, Shen A, Li Y, Zhuang Y, Lin K, Wu J, Liu J. Functionalized metal-organic framework-modified hydrogel that breaks the vicious cycle of inflammation and ROS for repairing of diabetic bone defects. Small. 2023;19:e2206919.
37. Gao S, Lv R, Hao N, Wang H, Lv Y, Li Y, Ji Y, Liu Y. Fabrication of pH/photothermal-responsive ZIF-8 nanocarriers loaded with Baicalein for effective drug delivery and synergistic chem-photothermal effects. Colloids Surf A. 2023;668:131401.
38. Xiang G, Wang B, Zhang W, Dong Y, Tao J, Zhang A, Chen R, Jiang T, Zhao X. A Zn-MOF-GOx-based cascade nanoreactor promotes diabetic infected wound healing by NO release and microenvironment regulation. Acta Biomater. 2024;182:245–59.
39. Xia X, Song X, Li Y, Hou W, Lv H, Li F, Li Y, Liu J, Li X. Antibacterial and anti-inflammatory ZIF-8@Rutin nanocomposite as an efficient agent for accelerating infected wound healing. Front Bioeng Biotechnol. 2022;10:1026743.
40. Tan S, Liu Z, Cong M, Zhong X, Mao Y, Fan M, Jiao F, Qiao H. Dandelion-derived vesicles-laden hydrogel dressings capable of neutralizing Staphylococcus aureus exotoxins for the care of invasive wounds. J Control Release. 2024;368:355–71.
41. Kermanian M, Nadri S, Mohammadi P, Iravani S, Ahmadi N, Alinezhad V, Shokrgozar MA, Haddad M, Mostafavi E, Maleki A. Zeolitic imidazolate frameworks: from bactericidal properties to tissue regeneration. J Control Release. 2023;359:326–46.
42. Liu T, Luo J, Bi G, Du Z, Kong J, Chen Y. Antibacterial synergy between linezolid and Baicalein against methicillin-resistant Staphylococcus aureus biofilm in vivo. Microb Pathog. 2020;147:104411.
43. Zhang Y, Tang Z, Chen L, Yang M, Zeng Y, Bai X, Zhang B, Zhou J, Zhang W, Tang S. Intelligent sequential degradation hydrogels by releasing bimetal-phenolic for enhanced diabetic wound healing. J Control Release. 2025;378:961–81.
44. Hernansanz-Agustín P, Enríquez JA. Generation of reactive oxygen species by mitochondria. Antioxid (Basel). 2021;10:415.
45. Qi XC, Li B, Wu WL, Liu HC, Jiang YP. Protective effect of Hyperoside against hydrogen peroxide-induced dysfunction and oxidative stress in osteoblastic MC3T3-E1 cells. Artif Cells Nanomed Biotechnol. 2020;48:377–83.
46. Zhang YF, Zhou L, Mao HQ, Yang FH, Chen Z, Zhang L. Mitochondrial DNA leakage exacerbates odontoblast inflammation through gasdermin D-mediated pyroptosis. Cell Death Discov. 2021;7:381.
47. Shao Z, Yin T, Jiang J, He Y, Xiang T, Zhou S. Wound microenvironment self-adaptive hydrogel with efficient angiogenesis for promoting diabetic wound healing. Bioact Mater. 2023;20:561–73.
48. Deng H, Liu Y, Shi Z, Yang J, Liu C, Mei X. Zinc regulates a specific subpopulation of VEGFA + microglia to improve the hypoxic microenvironment for functional recovery after spinal cord injury. Int Immunopharmacol. 2023;125:111092.
49. Zhang K, Lu J, Mori T, Smith-Powell L, Synold TW, Chen S, Wen W. Baicalin increases VEGF expression and angiogenesis by activating the ERR{alpha}/PGC-1{alpha} pathway. Cardiovasc Res. 2011;89:426–35.
50. Zhu J, Wang Z, Lv C, Li M, Wang K, Chen Z. Advanced glycation end products and health: A systematic review. Ann Biomed Eng. 2024;52:3145–56.
51. Yang Y, Huang S, Ma Q, Li N, Li R, Wang Y, Liu H. Combined therapeutic strategy based on blocking the deleterious effects of ages for accelerating diabetic wound healing. Regen Biomater. 2024;11:rbae062.
52. Xiao L, Wang N. PPAR-δ: A key nuclear receptor in vascular function and remodeling. J Mol Cell Cardiol. 2022;169:1–9.
53. Bougarne N, Weyers B, Desmet SJ, Deckers J, Ray DW, Staels B, De Bosscher K. Molecular actions of PPARα in lipid metabolism and inflammation. Endocr Rev. 2018;39:760–802.
54. Briganti S, Mosca S, Di Nardo A, Flori E, Ottaviani M. New insights into the role of PPARγ in skin physiopathology. Biomolecules. 2024;14.
55. Ju Z, Su M, Hong J, Kim E, Jung JH. Anti-inflammatory effects of an optimized PPAR-γ agonist via NF-κB pathway Inhibition. Bioorg Chem. 2020;96:103611.
56. Fu Q, Shen N, Fang T, Zhang H, Di Y, Liu X, Du C, Guo J. ACT001 alleviates inflammation and pyroptosis through the PPAR-γ/NF-κB signaling pathway in LPS-induced alveolar macrophages. Genes Genomics. 2024;46:323–32.
57. De Oliveira MR, Nabavi SF, Habtemariam S, Erdogan Orhan I, Daglia M, Nabavi SM. The effects of Baicalein and Baicalin on mitochondrial function and dynamics: A review. Pharmacol Res. 2015;100:296–308.
58. Zhang ZZ, Yu XH, Tan WH. Baicalein inhibits macrophage lipid accumulation and inflammatory response by activating the PPARγ/LXRα pathway. Clin Exp Immunol. 2022;209:316–25.
59. Zhou B, Jiang X, Zhou X, Tan W, Luo H, Lei S, Yang Y. GelMA-based bioactive hydrogel scaffolds with multiple bone defect repair functions: therapeutic strategies and recent advances. Biomater Res. 2023;27:86.

Publisher's note